INVESTIGATION ON THE TEMPERATURE DEPENDENT MECHANICAL BEHAVIOR OF A DUAL-PHASE MULTI-PRINCIPAL ELEMENT ALLOY WITH TRANSFORMATION INDUCED PLASTICITY

YASHAR M. SARDROUDI

ÖZYEĞİN UNIVERSITY

SEPTEMBER, 2025

INVESTIGATION ON THE TEMPERATURE DEPENDENT MECHANICAL BEHAVIOR OF A DUAL-PHASE MULTI-PRINCIPAL ELEMENT ALLOY WITH TRANSFORMATION INDUCED PLASTICITY

by

Yashar M. Sardroudi

Thesis

Submitted in Partial Fulfillment of the

Requirements for the Degree of

Master of science

in

Mechanical Engineering

Advisor: Prof. Dr. Güney Güven Yapıcı

Graduate School of Science and Engineering
Özyeğin University
İstanbul

September, 2025

INVESTIGATION ON THE TEMPERATURE DEPENDENT MECHANICAL BEHAVIOR OF A DUAL-PHASE MULTI-PRINCIPAL ELEMENT ALLOY WITH TRANSFORMATION INDUCED PLASTICITY

Approved by:

Prof. Dr. Güney Güven Yapıcı
Advisor
Department of Mechanical Engineering
Özyeğin University

Asst. Prof. Dr. Altuğ Başol
Department of Mechanical Engineering
Özyeğin University

Asst. Prof. Dr. Mehmet İpekoğlu
Department of Mechanical Engineering
Turkish-German University

Approval Date:

To the presence that made getting lost feel like a path, and confusion a place where answers wait.

DECLARATION OF ORIGINALITY

I hereby declare that I am the sole author of this thesis and that this is the true copy of my thesis, including the final revisions, approved by my thesis committee. All data and information have been obtained, produced, and presented in accordance with the rules of research ethics and principles of academic honesty. As required by these rules, to the best of my knowledge I have acknowledged ideas, thoughts, and any copyrighted material in accordance with the standard referencing rules. I certify that any part of this thesis has not been submitted for a degree or diploma in another educational institution.

Yashar M. Sardroudi

ABSTRACT

Multi-Principal Element Alloys (MPEAs), defined by their multi-component design and outstanding mechanical performance, are strong candidates for advanced structural applications. Among their strengthening mechanisms, transformation-induced plasticity (TRIP) is particularly significant under extreme temperatures. This study investigates the temperature-dependent TRIP effect in a heterogeneous dual-phase MPEA fabricated through thermomechanical processing. Homogenized single-phase face-centered cubic (FCC) samples initially showed ductile behavior without transformation. After post-cold rolling heat treatment, a dual-phase FCC + body-centered cubic (BCC) structure was obtained, enabling TRIP during deformation. Mechanical tests were conducted at −196 °C (cryogenic), 25 °C (room temperature), and 400 °C (elevated). While the FCC samples showed no phase change, the dual-phase microstructures displayed clear TRIP effects at cryogenic and room temperatures. At −196 °C, TRIP activity was most pronounced, producing an exceptional combination of ~1600 MPa ultimate tensile strength and ~18% elongation. This enhancement arises from deformation-induced martensitic transformations and the associated strain hardening. The findings confirm that thermomechanical processing can effectively tailor microstructural stability and optimize performance across temperatures.

Overall, this study provides insight into TRIP in heterogeneous MPEAs and highlights their potential for extreme environment applications while offering guidance for designing next-generation alloys with superior properties.

Keywords: MPEA, TRIP, Thermomechanical Processing, Cryogenic, Dual-phase

ÖZET

Çok Ana Elementli Alaşımlar (MPEA'lar), çok bileşenli tasarımları ve üstün mekanik özellikleri sayesinde ileri yapısal uygulamalar için güçlü adaylardır. Dayanım mekanizmaları arasında yer alan dönüşüm etkili plastisite (TRIP) özellikle aşırı sıcaklık koşullarında öne çıkmaktadır. Bu çalışma, termomekanik işlemlerle üretilmiş heterojen çift fazlı bir MPEA'da sıcaklığa bağlı TRIP etkisini incelemektedir. Başlangıçta homojenleştirilmiş tek fazlı yüzey merkezli kübik (YMK/FCC) numuneler, dönüşüm göstermeden sünek davranış sergilemiştir. Soğuk haddeleme sonrası ısıl işlem ile çift fazlı FCC + hacim merkezli kübik (HMK/BCC) yapı elde edilmiş ve deformasyon sırasında TRIP etkisi ortaya çıkmıştır. Mekanik testler -196 °C (kriyojenik), 25 °C (oda sıcaklığı) ve 400 °C (yüksek sıcaklık) koşullarında gerçekleştirilmiştir. FCC numunelerde faz dönüşümü gözlenmezken, çift fazlı mikro yapılar kriyojenik ve oda sıcaklığında belirgin TRIP davranışı sergilemiştir. -196 °C'de TRIP etkisi en yüksek seviyeye ulaşmış, numuneler yaklaşık 1600 MPa çekme dayanımı ve %18 kopma uzaması ile olağanüstü bir dayanım–süneklik dengesi göstermiştir. Bu iyileşme, deformasyon kaynaklı martenzitik dönüşümler ve buna bağlı şekil sertleşmesi ile açıklanmaktadır. Bulgular, termomekanik işlemlerin mikro yapısal kararlılığı düzenleyerek farklı sıcaklıklarda performansı optimize edebileceğini doğrulamaktadır.Sonuç olarak bu çalışma, heterojen MPEA'larda TRIP mekanizmasına dair kapsamlı bir bakış sunmakta, bu alaşımların farklı ortam sıcaklık koşullarındaki potansiyelini vurgulamakta ve üstün özelliklere sahip yeni nesil alaşımların tasarımına yol göstermektedir.

Anahtar Kelimeler: MPEA, TRIP, Termomekanik İşleme, Kriyojenik, Çift faz

ACKNOWLEDGEMENTS

I extend my deepest gratitude to my mother and father for their unconditional love, patience, and unwavering support throughout this journey.

My gratitude goes to my Nuni, whose presence and support in challenging times meant more than words can express.

To my dear friend Amin Radi, I am sincerely grateful for your companionship, encouragement, and the countless moments of laughter and motivation that lightened this challenging path.

I express my heartfelt thanks to my professor Güney Güven Yapıcı for their invaluable guidance, insightful feedback, and the knowledge they have shared, which has been pivotal in shaping the direction of this work.

TABLE OF CONTENT

DEDICATION ……... iv

DECLARATION OF ORIGINALITY ……... v

ABSTRACT ……... vi

ÖZET …….. vii

ACKNOWLEDGEMENTS ……... viii

LIST OF TABLES …….. xii

LIST OF FIGURES …… xiii

LIST OF ACRONYMS AND ABBREVIATIONS…… xiv

1. INTRODUCTION …….. 1

1.1 Background on High-Entropy Alloys (HEAs) …… 1

1.2 Importance of Transformation-Induced Plasticity (TRIP) …….. 3

1.3 Research Objectives and Scope …….. 4

2. LITERATURE REVIEW ……... 7

2.1 High-Entropy Alloys (HEAs) ……. 7

2.1.1 Definition and Concept of HEAs …….. 7

2.1.2 Configurational Entropy and Phase Stability in HEAs ……. 9

2.1.3 Benchmark HEA Systems ……. 11

2.2 Transformation-Induced Plasticity (TRIP) in HEAs …….. 13

2.2.1 Mechanism of TRIP in HEAs …… 13

2.2.2 Role of Temperature in TRIP Activation …….. 15

2.2.3 Stacking Fault Energy (SFE) and Alloy Design for TRIP ……. 17

2.3 Temperature Effects on Deformation Behavior …….. 20

2.3.1 Low-Temperature Behavior of FCC-Based HEAs …… 20

2.3.2 High-Temperature Deformation Behavior ……. 21

2.4 Compositionally Engineered HEAs …… 23

2.4.1 Elemental Effects on Phase Stability and Deformation ……. 23

2.4.2 Non-Equiatomic HEAs and Tailored TRIP Behavior ……... 25

2.5 Grain Structure and Dual-Phase Formation …… 27

2.6 Stacking Fault Energy and Its Role in Deformation Mechanisms of FCC-Based HEAs …… 29

2.7 Lattice Distortion and Atomic Size Mismatch in HEAs ……. 31

2.8 GNDs, TRIP Activation, and Summary of Literature Insights ……... 34

2.9 Summary of Literature Findings and Research Gaps ……. 36

2.9.1 Key Insights from Previous Studies …….. 36

3. MATERIALS AND METHODS……. 39

3.1 Alloy Design and Fabrication ……. 39

3.1.1 Selection of Elements and Design Rationale ……. 39

3.1.2 Alloy Melting, Casting, and Homogenization ……... 42

3.2 Thermomechanical Processing ……... 44

3.2.1 Cold Rolling Procedure ……. 44

3.2.2 Post-Deformation Annealing Treatments …….. 45

3.3 Microstructural Characterization …… 46

3.3.1 Pre- and Post-Tensile Test Analysis via XRD and EBSD ……. 46

3.4 Mechanical Testing …… 48

3.4.1 Tensile Testing Setup and Parameters ……... 48

3.4.2 Mechanical Behavior at Cryogenic, Room, and Elevated Temperatures 49

4. RESULTS AND DISCUSSION ……. 51

4.1 Mechanical Properties at Varying Temperatures …… 51

4.2 Phase Transformation Behavior Across Temperatures …….. 53

4.3 EBSD-Based Strain and Dislocation Analysis ……... 58

4.4 Discussion on TRIP Activation Mechanisms …… 63

4.5 Correlation Between Microstructure and Mechanical Behavior …… 66

4.6 Strain Hardening Behavior ……..…… 68

5. CONCLUSION AND FUTURE WORK ……... 71

REFERENCES ……... 73

LIST OF TABLES

Table 2.1: Typical mechanical properties of the Cantor alloy ……. 12

Table 1.2: Effect of temperature on SFE, deformation mechanisms, and TRIP activity in the studied HEA ……. 16

Table 2.2: Summary of yield strength, tensile strength, and ductility of selected FCC-based HEAs at 77 K, illustrating the effect of composition on cryogenic mechanical performance ……. 21

Table 2.4: Influence of composition on stacking fault energy (SFE) and dominant deformation mechanisms in FCC-based high-entropy alloys at room and cryogenic temperatures ……. 30

Table 3.1: post deformation phase transformation fractions of annealed samples …… 54

LIST OF FIGURES

Figure 2.1: Conceptual Difference Between Conventional Alloys (a) and High Entropy Alloys (b)……... 7

Figure 2.2: Effect of Number of Elements on Configurational Entropy ……... 11

Figure 1.3: Ashby plot of fracture toughness vs. yield strength for HEAs, conventional alloys, and other materials, with dashed lines and phase structures (FCC, BCC, dual phase) indicated for comparison ……. 13

Figure 2.4: Schematic illustration of TRIP mechanism in HEAs showing phase transformation from FCC to HCP during deformation ……. 15

Figure 2.5: Temperature-Dependent Deformation Mechanism Map Showing Transition from TRIP to TWIP to Dislocation Slip …… 17

Figure 2.6: Deformation mechanisms in FCC alloys as a function of stacking fault energy, showing transitions from dislocation glide to twinning and TRIP. 19

Figure 2.7: Qualitative effect of key alloying elements on stacking fault energy (SFE), FCC phase stability, and TRIP tendency in FCC-based HEAs. Negative SFE values indicate a reduction that promotes TRIP, while positive values suggest suppression. Phase stability reflects FCC retention, and TRIP tendency shows each element's influence on transformation-induced plasticity…… 25

Figure 3.1: (a and b) True stress/strain and (c and d) strain hardening rate plots for the as-received (a and c) and annealed (b and d) conditions during tensile testing at -196, +25, and 400°C. ……. 53

Figure 3.2: (a and b) XRD spectra, EBSD results for (c and g) phase maps, (d and h) inverse pole figure (IPF) maps, (e and i) kernel average misorientation (KAM) maps, (f and j) geometrically necessary dislocation (GND) 10^{12} m^{-2} maps for the as-received and annealed samples, respectively. …… 55

Figure 3.3: XRD spectra after deformation at cryogenic and high temperatures; a) for the as-received sample and b) for the annealed sample. …… 58

Figure 3.4: EBSD results of the annealed condition for deformation at varying temperatures; (a, e and i) phase maps, (b, f and j) IPF maps, (c, g and k) KAM maps, (d, h and l) GND 10^{12} m^{-2} maps. …… 60

Figure 3.5: EBSD results of the as-received condition for deformation at varying temperatures; (a, e, i) phase maps, (b, f, j) IPF maps, (c, g and k) KAM maps, (d, h, l) GND 10^{12} m^{-2} maps. ……. 62

LIST OF ACRONYMS AND ABBREVIATIONS

MPEA: Multi Principal Element Alloy

HEA: High Entropy Alloy

FCC: Face Centered Cubic

BCC: Body Centered Cubic

HCP: Hexagonal Close Packed

SFE: Stacking Fault Energy

IPF: Inverse Pole Figures

KAM: Kernel Average Misorientation

GND: Geometrically Necessary Dislocations

SHR: Strain Hardening Rate

XRD: X-ray Diffraction

SEM: Scanning Electron Microscopy

TEM: Transmission Electron Microscopy

DED: Directed Energy Deposition

SLM: Selective Laser Melting

UTS: Ultimate Tensile Strength

YS: Yield Strength

FESEM: Field Emission Scanning Electron Microscopy

EBSD: Electron Backscatter Diffraction

DFT: Density Functional Theory

EDM: Electrical Discharge Machining

TWIP: Twinning-Induced Plasticity

SSD: Statistically Stored Dislocations

GNB: Geometrically Necessary Boundaries

AM: Additive Manufacturing

1. INTRODUCTION

1.1 Background on High Entropy Alloys (HEAs)

The development of high-entropy alloys (HEAs) marks a paradigm shift in the field of alloy design and materials science. Traditionally, engineering alloys have been formulated based on one or two principal elements, with other alloying elements added in small quantities to modify specific properties. While this method has yielded many successful materials such as stainless steels, superalloys, and titanium alloys it also imposes inherent compositional limitations. In contrast, the concept of HEAs introduced by Yeh et al. in 2004 [1]. challenged this convention by proposing the deliberate use of multiple principal elements in equiatomic or near-equiatomic ratios. This radical approach results in a high configurational entropy, which, under appropriate processing conditions, stabilizes simple solid solution phases (typically FCC or BCC), rather than complex and brittle intermetallic compounds.

This high entropy strategy gives rise to a range of novel phenomena collectively referred to as the "core effects" of HEAs: high configurational entropy, sluggish diffusion, severe lattice distortion, and the cocktail effect. Each of these effects contributes to the unique physical and mechanical behavior observed in HEAs. For instance, severe lattice distortion arising from atomic size mismatch among constituent elements can impede dislocation motion and enhance strength, while sluggish diffusion slows down microstructural degradation mechanisms such as grain growth and phase separation at elevated temperatures [2]. The cocktail effect, although not yet fully

understood, suggests that the synergistic interaction among multiple elements can result in unexpected and often beneficial properties not achievable in conventional alloys.

As a result of these unique effects, HEAs exhibit a rare combination of high strength, ductility, fatigue resistance, wear resistance, and thermal stability, positioning them as promising candidates for applications in extreme environments. In particular, their ability to retain toughness and fracture resistance at cryogenic temperatures makes them attractive for use in aerospace structures, liquefied gas containment, and deep-space exploration systems [3]. The equiatomic CoCrFeMnNi alloy often referred to as the Cantor alloy is the most extensively studied HEA and has become the benchmark system for investigating fundamental deformation mechanisms. Numerous studies have demonstrated its impressive balance of mechanical properties across a wide temperature range, highlighting the potential of HEAs to meet performance demands where conventional alloys fall short.

Furthermore, the chemical complexity of HEAs also contributes to their excellent resistance to oxidation and corrosion. The presence of multiple elements in high concentrations promotes the formation of protective oxide scales and passive layers, even in aggressive environments. These features broaden their appeal for applications not only in structural systems but also in energy and chemical industries where materials are frequently exposed to corrosive agents and temperature fluctuations. As the field matures, it is increasingly clear that the performance of HEAs is not only a result of composition but also of processing history, microstructural design, and the active deformation mechanisms they engage under service conditions.

1.2 Importance of Transformation-Induced Plasticity (TRIP)

One of the most compelling deformation mechanisms enhancing the mechanical performance of certain HEAs is transformation-induced plasticity (TRIP). The TRIP mechanism, originally observed in advanced steels, involves a stress or strain driven transformation from a ductile, metastable parent phase typically FCC into a harder and often more brittle secondary phase, such as BCC (α′ martensite) or HCP (ε martensite), during plastic deformation. This transformation absorbs mechanical energy and contributes to sustained strain hardening, thereby improving the strength–ductility synergy that is often difficult to achieve in metallic systems [4].

In the context of HEAs, the TRIP mechanism has garnered significant attention for its ability to further enhance already impressive mechanical properties. The effectiveness of TRIP in HEAs depends critically on factors such as temperature, Stacking Fault Energy (SFE), phase stability, and microstructural heterogeneity. At low temperatures, SFE tends to decrease, which suppresses cross-slip and promotes partial dislocation activity, mechanical twinning, and martensitic transformation [5]. These microstructural changes provide additional deformation pathways and barriers to dislocation motion, resulting in increased work hardening and delayed necking. Experimental studies have shown that TRIP activated HEAs exhibit superior mechanical properties at cryogenic temperatures, including ultimate tensile strengths above 1.5 GPa and elongations exceeding 15%, making them strong contenders for structural applications in low-temperature environments [6].

However, TRIP is not confined to cryogenic conditions. With proper thermomechanical processing such as cold deformation followed by controlled annealing

it is possible to engineer a dual-phase microstructure where the metastable FCC matrix is predisposed to transform under strain, even at room or moderately elevated temperatures [7,8]. Grain size refinement, dislocation substructure, and pre-existing BCC nuclei can all influence the onset and kinetics of transformation. This controllability opens new pathways for designing HEAs tailored for application-specific environments. For instance, materials used in rocket propulsion systems, LNG tanks, or turbine blades may benefit from TRIP mechanisms activated under diverse thermal and mechanical loads.

Moreover, the interaction of TRIP with other deformation mechanisms such as dislocation slip, twinning-induced plasticity (TWIP), and dynamic recrystallization offers a complex yet tunable response that can be harnessed through careful alloy design and processing. In dual-phase HEAs, where hard and soft regions coexist, the TRIP effect can be further amplified due to stress partitioning and back-stress generation, resulting in higher work hardening rates and improved overall ductility. As such, the TRIP mechanism not only enhances mechanical properties but also expands the functional versatility of HEAs across a wide operational spectrum.

1.3 Research Objectives and Scope

The overarching aim of this research is to systematically investigate the effect of temperature on the activation and effectiveness of the TRIP mechanism in high-entropy alloys with dual-phase microstructures. Specifically, the study focuses on understanding how thermomechanical processing namely homogenization, cold rolling, and annealing affects phase stability, dislocation structure, and the extent of strain-induced

transformation under different thermal conditions. To this end, a high-entropy alloy based on the equiatomic CoCrFeMnNi system was subjected to a sequence of treatments to produce two distinct microstructural states: a homogenized FCC single phase matrix (as-received condition), and a dual phase FCC BCC structure (annealed condition). These samples were then subjected to uniaxial tensile testing at three representative temperatures: −196 °C (cryogenic), +25 °C (ambient), and +400 °C (elevated). This temperature range was chosen to simulate a broad spectrum of application environments and to provide insights into temperature-sensitive deformation and transformation behaviors.

The research is guided by several key questions aimed at understanding the deformation behavior of TRIP-active High-Entropy Alloys (HEAs). One central question is how deformation temperature influences the onset, rate, and completeness of the FCC to BCC phase transformation. Additionally, the study explores the roles of (SFE), dislocation density, and grain size in governing phase stability and transformation kinetics. A further point of inquiry considers whether microstructural heterogeneity can be deliberately engineered to enhance TRIP activity, thereby achieving an improved balance between strength and ductility in these complex alloys. Initial experimental results indicate that the annealed condition exhibits superior mechanical performance at cryogenic temperatures, reaching ultimate tensile strengths above 1600 MPa and elongations approaching 18%. This behavior is attributed to a synergistic effect of phase transformation, grain boundary strengthening, and dislocation-mediated hardening. EBSD and XRD analyses confirm that the FCC to BCC transformation is more active at lower temperatures, correlating strongly with a decrease in SFE and an increase in dislocation storage particularly geometrically necessary dislocations (GNDs).

This work therefore aims not only to clarify the microstructural mechanisms underpinning TRIP in HEAs but also to offer practical guidance for alloy design and processing routes. By integrating experimental findings with theoretical insights from the literature, this study contributes to the broader goal of developing next-generation structural materials that combine adaptability, robustness, and high performance across extreme service conditions.

2. LITERATURE REVIEW

2.1 High-Entropy Alloys (HEAs)

2.1.1 Definition and Concept of HEAs

HEAs represent a paradigm shift in the field of metallurgy, diverging from the century-old principles that traditionally centered around one or two principal elements with minor additions of alloying elements. Instead, HEAs are composed of five or more elements in near-equiatomic ratios, generally each constituting between 5 and 35 atomic percent. This radical design concept was first proposed in the early 2000s and has since catalyzed a significant wave of research aimed at exploring previously uncharted compositional territories. Figure shows a conceptual atomic structure difference between Conventional alloys and High Entropy Alloys [9].

Figure 2.1: *Conceptual Difference Between Conventional Alloys (a) and High-Entropy Alloys (b)*

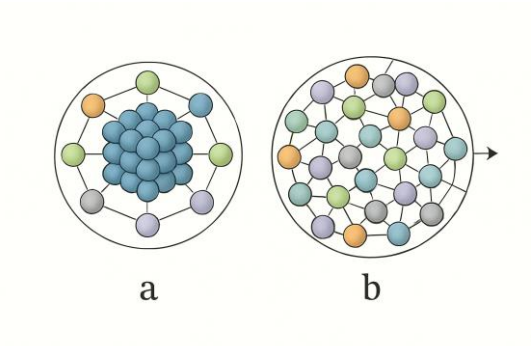

What distinguishes HEAs from conventional alloys is not just their complex chemical makeup, but also the unexpected simplicity of their resulting microstructures. Despite the vast number of possible atomic arrangements, HEAs tend to form simple solid solution phases typically face centered cubic (FCC), body centered cubic (BCC), or hexagonal close packed (HCP) instead of complicated intermetallic compounds. This phenomenon arises due to a set of unique and synergistic effects, particularly high configurational entropy, which contributes to the stability of solid solution phases over intermetallics, even under equilibrium conditions [10].

The term "high entropy" stems from the configurational entropy of mixing (S_{config}), which is derived from Boltzmann's equation:

$$S_{config} = -R \sum_{i=1}^{n} x_i \ln x_i \tag{2.1}$$

Here, R is the universal gas constant, x_i is the atomic fraction of the i^{th}element, and n is the total number of principal elements. In an equiatomic five-element alloy, the configurational entropy reaches about $1.61R$, which is substantially higher than that of traditional alloys. This elevated entropy reduces the Gibbs free energy ($G = H - TS$) and stabilizes disordered solid solutions, particularly at high temperatures [11].

This design flexibility allows for the exploration of vast compositional spaces. The implication is profound: whereas traditional alloy development exploits a minute fraction of the potential alloying universe, HEAs unlock an almost limitless palette for materials scientists to tailor mechanical, thermal, magnetic, and chemical properties [12]. Over the last two decades, research has shown that HEAs can outperform conventional alloys in numerous aspects, such as strength-ductility trade-offs, high-temperature

softening resistance, corrosion resistance, and even radiation tolerance [13,14]. These promising attributes are particularly advantageous for extreme environments such as cryogenic storage systems, nuclear reactors, aerospace engines, and even biomedical implants.

2.1.2 Configurational Entropy and Phase Stability in HEAs

One of the foundational principles that make high-entropy alloys (HEAs) distinct from conventional alloys is their thermodynamic stability, which is largely attributed to high configurational entropy. In multicomponent systems with near-equiatomic proportions, configurational entropy becomes a dominant factor influencing phase stability, favoring the formation of disordered solid solutions over ordered intermetallic compounds or multiphase microstructures.

In statistical thermodynamics, the configurational entropy of mixing is described by:

$$S_{config} = -R \sum_{i=1}^{n} x_i \ln x_i \tag{2.2}$$

In this equation, R represents the universal gas constant with a value of (8.314 $J \cdot mol^{-1} \cdot K^{-1}$). The term x_i denotes the atomic fraction of the i^{th} element in the alloy system, while n refers to the total number of constituent elements present in the composition. For a perfectly equiatomic alloy with n components, this simplifies to:

$$S_{config} = R \ln n \tag{2.3}$$

This means an equiatomic 5-component system, such as CrMnFeCoNi, has $S_{config} \approx 1.61R$, which classifies it as a high-entropy alloy. For comparison, a ternary alloy yields about $1.10R$, often classified as a medium-entropy alloy (MEA). The Gibbs free energy of mixing governs the stability of any alloy phase:

$$(\Delta G = \Delta H - T\Delta S) \tag{2.4}$$

In this expression, ΔG represents the change in Gibbs free energy, ΔH is the enthalpy of mixing, T denotes the absolute temperature, and ΔS refers to the entropy of mixing.

In HEAs, the relatively high value of ΔS reduces ΔG, especially at elevated temperatures, stabilizing simple disordered FCC or BCC solid solutions and suppressing the formation of complex intermetallic phases. However, entropy is not the only factor; enthalpy of mixing ΔH and atomic size mismatch also play critical roles. If the enthalpy is excessively negative, or atomic sizes diverge significantly, phase separation or formation of intermetallics may still occur, despite the high entropy [15]. It is important to recognize that while configurational entropy contributes to phase stability, it does not universally prevent the formation of multiple phases. Numerous HEAs exhibit dual or multi-phase microstructures, especially at lower temperatures. Therefore, modern researchers increasingly consider entropy as one of several design parameters, not the sole defining criterion. Recent studies also highlight the significance of sluggish diffusion, lattice distortion, and the cocktail effect in controlling the thermodynamics and kinetics of phase evolution. In Figure 2.2 the effect of number of elements in a composition on the configurational entropy has been demonstrated.

Figure 2.2: *Effect of Number of Elements on Configurational Entropy* [16]

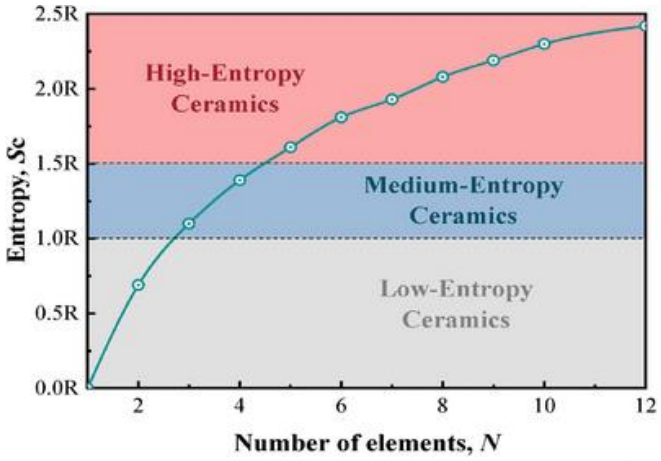

2.1.3 Benchmark HEA Systems

Since the advent of the high-entropy alloy concept, several benchmark systems have emerged that serve as foundational references in both academic research and industrial development. These alloys are chosen for their well-documented phase behavior, mechanical response, and thermodynamic properties. Among them, the most widely studied is the equiatomic CrMnFeCoNi alloy, commonly referred to as the Cantor alloy, named after Professor Brian Cantor, who first reported it [17]. The Cantor alloy crystallizes as a single-phase FCC solid solution and is known for its exceptional combination of ductility and strength, particularly at cryogenic temperatures. What sets it apart is its ability to maintain its toughness and avoid brittle fracture even down to liquid nitrogen temperatures (−196 °C). This behavior is partially attributed to its relatively low SFE, which promotes planar slip, mechanical twinning, and TRIP (Transformation Induced Plasticity) mechanisms at low temperatures [18]. Table 2.1 shows the typical mechanical properties of the Cantor alloy:

Table 2.1: *Typical mechanical properties of the Cantor alloy:*

CONTOR Alloy	Yield Strength (MPa)	Ultimate Tensile Strength (MPa)	Elongation (mm/mm)
RT	~200–300	~700–750	~50%
Cryo	rising to 700+	up to 1000+	~30%

This balance of strength and ductility has made the Cantor alloy a model system for studies in deformation mechanisms, grain boundary behavior, and microstructural evolution. Another significant benchmark system is the AlxCoCrFeNi family, where the aluminum content is systematically varied. Aluminum has a strong effect on both phase formation and mechanical behavior. At low Al content ($x < 0.5$), the alloy tends to remain FCC, but higher Al concentrations lead to BCC or B2 phases, introducing increased strength at the cost of ductility. These alloys show how composition manipulation within a HEA framework allows tailoring of properties through microstructural control [19]. For high temperature applications, refractory element based HEAs (e.g., NbMoTaW, HfNbTaTiZr) have garnered attention due to their superior strength retention above 1000 °C. These alloys are predominantly BCC solid solutions, formed from elements with high melting points and low mutual solubility in conventional systems. However, these alloys often suffer from room-temperature brittleness, which is an ongoing research challenge [20].

A sub-classification of HEAs, medium entropy alloys (MEAs), such as CrCoNi, have shown impressive toughness and strain hardening behavior. While containing only three principal elements, MEAs still maintain significant configurational entropy and demonstrate many of the same beneficial effects (e.g., low SFE, delayed necking, and cryogenic ductility). The CrCoNi alloy, for instance, has been reported to achieve fracture

toughness exceeding 200 MPa√m at cryogenic temperatures [21]. he mechanical property space of HEAs in relation to conventional alloys and other materials is illustrated in the Ashby plot of fracture toughness versus yield strength (Figure 2.3).

Figure 2.3: *Ashby plot of fracture toughness vs. yield strength for HEAs, conventional alloys, and other materials, with dashed lines and phase structures (FCC, BCC, dual phase) indicated for comparison* [22]

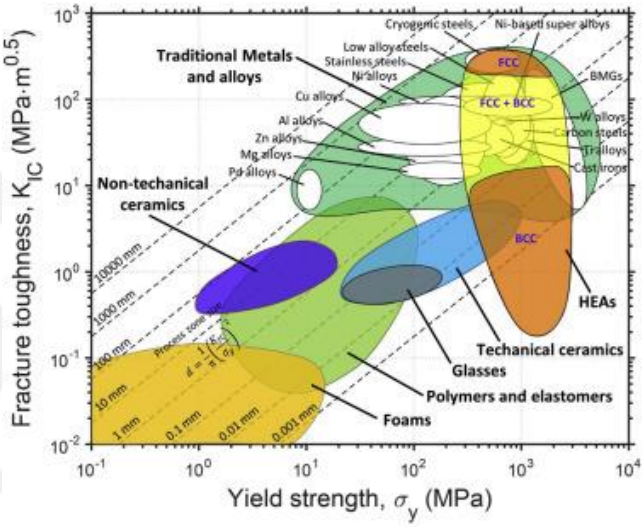

2.2 Transformation-Induced Plasticity (TRIP) in HEAs

2.2.1 Mechanism of TRIP in HEAs

Transformation-Induced Plasticity (TRIP) is a deformation mechanism in which a parent phase typically FCC in HEAs transforms into a secondary phase (commonly HCP or BCC) under the influence of mechanical stress or strain (See Figure 2.4). In high entropy alloys, especially those with metastable FCC structures and low SFE, this phenomenon plays a crucial role in enhancing strength, ductility, and strain-hardening [23]. Unlike slip or twinning, TRIP contributes to plasticity by consuming deformation energy in the form of phase transformation, which acts as a barrier to crack propagation

and promotes strain delocalization. During tensile loading, the metastable FCC grains undergo a stress-assisted martensitic transformation, generally into HCP (especially in CrMnFeCoNi-type alloys). This newly formed HCP phase has higher strength but lower ductility, and its presence helps pin dislocations, strengthen the microstructure, and delay failure [24].

The transformation typically begins at grain boundaries, twin intersections, or stress concentration zones. With increasing strain, the transformed phase grows along shear planes, creating a dual-phase microstructure. This microstructural evolution contributes to work hardening, thereby improving tensile ductility and delaying necking [25]. Mathematically, this mechanism can be evaluated by considering the Gibbs free energy difference between the FCC and the HCP phases:

$$\Delta G_{FCC \rightarrow HCP} = G_{HCP} - G_{FCC} \tag{2.5}$$

When $\Delta G < 0$, the transformation becomes energetically favorable. However, the energy barrier must be overcome by mechanical work, meaning that deformation is necessary to initiate the transformation [26].

Figure 2.4: *Schematic illustration of TRIP mechanism in HEAs showing phase transformation from FCC to BCC during deformation.*

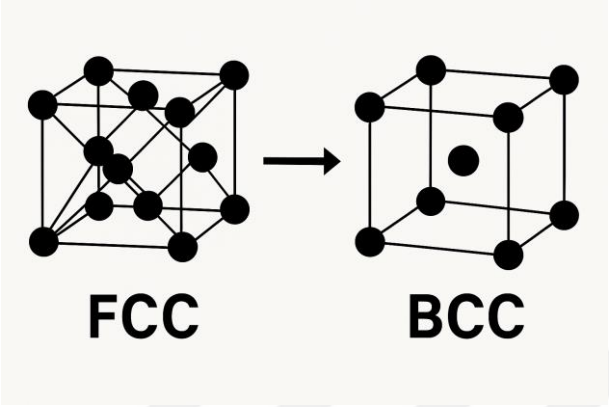

2.2.2 Role of Temperature in TRIP Activation

The efficiency and extent of transformation-induced plasticity (TRIP) in high-entropy alloys (HEAs) are strongly influenced by temperature, making it a key parameter in governing phase transformation mechanisms. Changes in temperature affect the SFE, the critical stress required for transformation, and the alloy's overall mechanical response factors that collectively determine the onset and intensity of TRIP behavior [27]. At cryogenic or sub-zero temperatures, such as −196 °C, the SFE in FCC-based HEAs decreases substantially. This promotes the formation of stacking faults, which act as nucleation sites for martensitic phase transformations (e.g., FCC to HCP or BCC). Under plastic deformation, these conditions favor the activation of TRIP, enhancing strain hardening and delaying necking. Studies on metastable systems like the Cantor alloy have consistently shown that low temperatures amplify the TRIP effect, leading to improved mechanical performance, as detailed in Table. The increased transformation activity at

these temperatures also contributes to enhanced fracture resistance by distributing strain more uniformly throughout the microstructure [28–30].

Table 2.2: *Effect of temperature on SFE, deformation mechanisms, and TRIP activity in the studied HEA.*

Temperature	SFE Behavior	Dominant Mechanism	TRIP Activity	UTS (MPa)
−196 °C	Very Low	FCC → HCP TRIP + twins	High	~1300–1400
25 °C	Low to Mid	Dislocation slip + minor TRIP	Moderate	~600–800
>400 °C	High	Dislocation creep/recovery	Negligible	<500

At room temperature, TRIP remains active in many HEAs, but its effect is less pronounced. Higher SFE values make dislocation glide the dominant deformation mechanism, and phase transformation occurs only in compositions with sufficient metastability. The FCC phase tends to remain stable, with limited transformation to HCP or BCC structures [31]. As the temperature rises further, typically into the range of 400–600 °C, the SFE increases significantly, effectively suppressing both twinning and phase transformation. In this regime, deformation is primarily accommodated by dislocation glide and thermally activated processes such as dynamic recovery. The FCC matrix becomes increasingly stable, and TRIP activity diminishes or becomes entirely inactive. Figure 2.5 illustrates the temperature-dependent evolution of deformation mechanisms, showing the transition from transformation-induced plasticity (TRIP) at low temperatures to twinning-induced plasticity (TWIP) and ultimately to dislocation slip at elevated temperatures [32].

Figure 2.5: *Temperature-Dependent Deformation Mechanism Map Showing Transition from TRIP to TWIP to Dislocation Slip* [32]

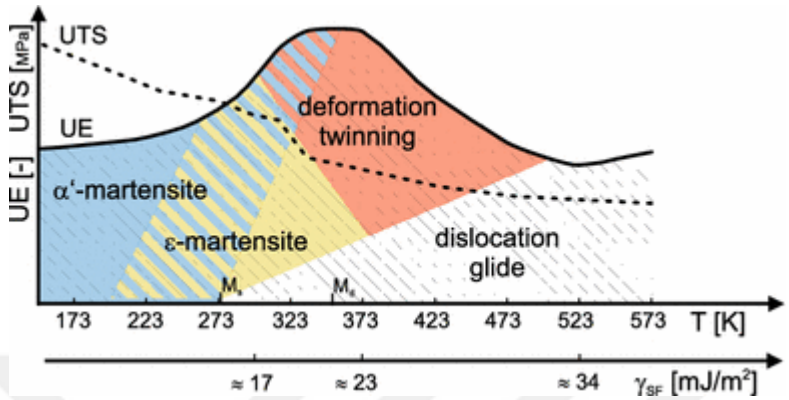

2.2.3 Stacking Fault Energy (SFE) and Alloy Design for TRIP

SFE is a fundamental property that governs the dominant deformation mechanisms in face centered cubic (FCC) high-entropy alloys (HEAs). It plays a decisive role in determining whether deformation is carried by dislocation glide, mechanical twinning (TWIP), or transformation-induced plasticity (TRIP) [33]. In TRIP-active HEAs, low SFE values typically below 20 mJ/m² facilitate partial dislocation motion and promote the nucleation of hexagonal close packed (HCP) or body centered cubic (BCC) phases from the parent FCC structure under applied stress. These phase transformations significantly enhance strain hardening by introducing new interfaces that obstruct dislocation motion and accommodate plastic deformation [28].

The deformation mechanisms in face centered cubic (FCC) alloys are strongly influenced by their SFE. When the SFE exceeds 40 mJ/m², dislocation glide becomes the dominant mode of deformation, with minimal contribution from twinning or

transformation-induced plasticity (TRIP). In the intermediate range of 20-40 mJ/m², twinning-induced plasticity (TWIP) governs the deformation behavior. However, when the SFE drops below 20 mJ/m², TRIP becomes the prevailing mechanism, typically involving phase transformations from FCC to either hexagonal close-packed (HCP) or body centered cubic (BCC) structures. Low SFE reduces the energy cost of forming stacking faults, allowing them to accumulate and act as nucleation sites for secondary phases. This makes low SFE alloys particularly attractive for high-strength, high-ductility applications.

High-Entropy Alloy (HEA) compositions can be strategically tailored to achieve specific SFEs that activate desired deformation mechanisms. Several alloying elements have a significant impact on SFE. For instance, manganese (Mn) and cobalt (Co) are known to reduce SFE and promote the formation of hexagonal close-packed (HCP) phases. Chromium (Cr), while stabilizing the face centered cubic (FCC) phase, also contributes to lowering SFE when combined with certain other elements. In contrast, nickel (Ni) and aluminum (Al) generally increase SFE, which suppresses twinning and transformation-induced plasticity (TRIP), and may also stabilize body centered cubic (BCC) phases. Additionally, interstitial elements such as carbon (C), nitrogen (N), and boron (B) are effective in lowering SFE and enhancing the alloy's strain hardening capacity.

For instance, the equiatomic CrMnFeCoNi alloy often used as a reference HEA has an estimated SFE of 18–22 mJ/m² at room temperature, a value low enough to support TRIP. At cryogenic temperatures, this value decreases even further, intensifying the transformation behavior. Modified compositions like CrCoNi, which contain reduced

amounts of Mn and Fe, show even lower SFE values around 14 mJ/m², resulting in more pronounced TRIP effects and higher work-hardening capability [34,35]. Empirical and first-principles models have been developed to predict SFE in HEAs based on electronegativity, mixing enthalpy, and atomic radius mismatch. One widely used formula to estimate atomic size mismatch (δ) is:

$$\delta = \sqrt{\sum_{i=1}^{n} c_i \left(1 - \frac{r_i}{\bar{r}}\right)^2} \tag{2.6}$$

In this formulation, c_i denotes the atomic percentage of the i^{th} element, r_i represents the atomic radius of the i^{th} element, and $\bar{r}$ is the average atomic radius of the alloy. A lower atomic size difference parameter (δ) is typically associated with a reduced SFE, which in turn enhances the activation of TRIP (See Figure 2.6).

Figure 2.6: *Deformation mechanisms in FCC alloys as a function of stacking fault energy, showing transitions from dislocation glide to twinning and TRIP* [17,36]

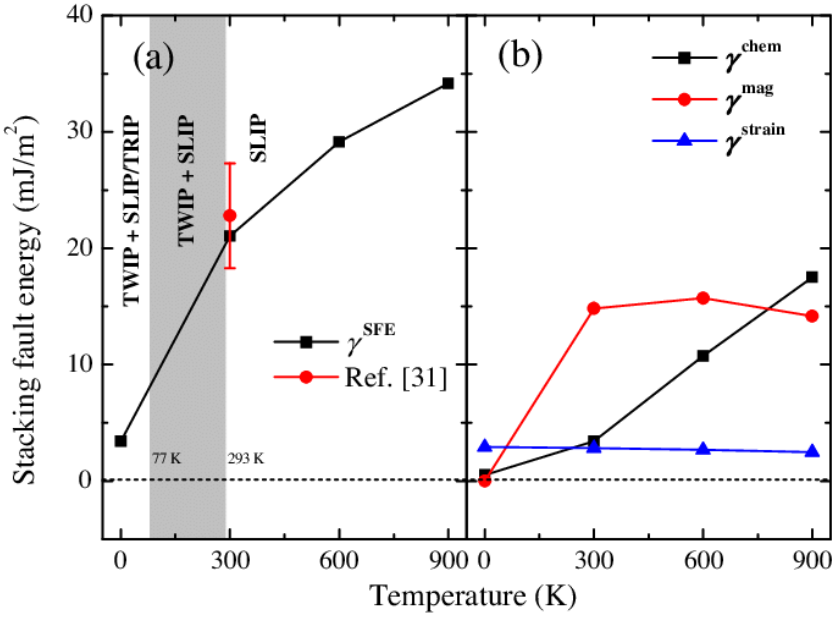

2.3 Temperature Effects on Deformation Behavior

2.3.1 Low Temperature Behavior of FCC Based HEAs

FCC based high entropy alloys (HEAs), such as CrCoNi and its derivatives, exhibit outstanding mechanical performance at cryogenic temperatures, making them promising materials for applications in aerospace, cryogenic storage, space structures, and liquefied gas containers. Unlike traditional alloys, these HEAs do not become brittle at low temperatures. Instead, they demonstrate a unique enhancement in both strength and ductility a rare and highly valuable combination in structural materials [31,37]. At cryogenic temperatures (e.g., −196 °C), FCC-based HEAs undergo a substantial increase in yield strength (YS) and ultimate tensile strength (UTS) while maintaining significant ductility (See Table 2.3). This improvement is primarily attributed to the activation of transformation-induced plasticity (TRIP) and twinning-induced plasticity (TWIP) mechanisms, which are suppressed at higher temperatures due to increased stacking fault energy (SFE) [38,39].

At low temperatures, the SFE decreases, which facilitates the formation of partial dislocations, stacking faults, and transformation to the body centered cubic (BCC) phase. Additionally, dynamic recovery processes are suppressed, leading to dislocation pile-up and enhanced work hardening. Under these conditions, transformation-induced plasticity (TRIP) becomes active due to the reduced thermal stability of the face centered cubic (FCC) phase, resulting in stress-assisted FCC to HCP or BCC transformations. Deformation is further characterized by planar slip, which dominates because of limited cross-slip, thereby delaying the onset of necking and promoting more uniform plastic

flow. Collectively, these effects produce a synergistic deformation mode that combines dislocation glide, twinning, and TRIP culminating in exceptional fracture toughness.

Table 2.3: *Summary of yield strength, tensile strength, and ductility of selected FCC-based HEAs at 77 K, illustrating the effect of composition on cryogenic mechanical performance.*

Alloy Composition	Temperature (K)	Yield Strength (MPa)	Ultimate Tensile Strength (MPa)	Elongation (%)	Reference
CrCoNi	77	~850	>1300	~90	[40]
FeCoCrNi	77	~716	—	~17.4	[41]
$CrCoNiSi_{0.3}$	77	980	1800	62	[37]
Fe-based HEA	77	1325	1446	—	[42]
$Fe_{40}Mn_{20}Cr_{20}Ni_{20}$	77	438	676	32	[43]
$Co_{50}Cr_{20}Ni_{20}Fe_5Mn_5$	77	502	1002	50	[44]
NiCoV	77	841–1400	1434–1890	23–47	[45]
CrCoNi (heterostructured)	77	1244	—	34	[39]
$Al_{0.3}CoCrFeNi$	77	600	1100	30	[46]
$CoCrFeNiMo_{0.5}$	77	700	1200	40	[47]
$CoCrFeNiCu_{0.5}$	77	550	1000	45	[48]
$CoCrFeNiNb_{0.2}$	77	800	1300	25	[49]

2.3.2 High Temperature Deformation Behavior

While FCC based HEAs demonstrate outstanding mechanical performance at cryogenic temperatures, their behavior at elevated temperatures presents a different set of challenges. Above moderate temperatures typically beyond 400 °C these alloys, particularly single-phase systems like CrMnFeCoNi and CrCoNi, tend to experience a decline in mechanical strength despite retaining good phase stability and oxidation resistance. Understanding their thermal softening behavior and resistance to creep is critical for enabling their use in high-temperature applications such as aerospace components, power systems, and thermal barriers [27,50]. As temperature increases, the SFE also rises, which progressively suppresses twinning and transformation-induced

plasticity (TWIP and TRIP). As a result, dislocation slip becomes the dominant deformation mechanism. This is further aided by thermally activated processes like cross slip and dislocation climb, which enhance dislocation mobility but also reduce the alloy's strain-hardening ability. The net effect is a softening response, marked by decreased yield strength and a tendency toward premature plastic instability [51,52].

The high-temperature mechanical response of these alloys is governed not only by dislocation dynamics but also by microstructural changes. Processes such as grain growth, dynamic recrystallization, and in some cases, grain boundary sliding, can significantly affect their deformation behavior. This is especially evident in fine-grained microstructures, which are more susceptible to creep under thermal stress. Although many FCC based HEAs maintain a stable solid-solution structure up to relatively high temperatures, long-term thermal exposure can lead to structural degradation. This includes grain coarsening, the precipitation of intermetallic compounds, and the formation of secondary BCC phases, particularly in systems with complex chemistries or specific alloying elements like Al, Ti, or Nb [46,49,53]. To enhance their high-temperature stability, researchers have explored alloying strategies aimed at strengthening the matrix and inhibiting detrimental microstructural changes. These include the incorporation of elements that promote stable precipitate formation for dispersion strengthening, or the development of refractory HEAs (RHEAs) that leverage elements like Mo, Nb, Ta, and W [54–56]. While these strategies improve performance at elevated temperatures, they often involve trade-offs, such as reduced ductility or increased brittleness at room temperature.

2.4 Compositionally Engineered HEAs

2.4.1 Elemental Effects on Phase Stability and Deformation

The mechanical behavior of high-entropy alloys (HEAs) is strongly influenced by the role of each constituent element, particularly in terms of their effects on phase stability, SFE, and dominant deformation mechanisms such as dislocation slip, mechanical twinning, and transformation-induced plasticity (TRIP). Even minor variations in elemental composition can lead to significant differences in mechanical performance, especially across various temperature regimes [49,57,58].

Manganese (Mn) plays a pivotal role in activating both TRIP and TWIP by significantly lowering the SFE. Its presence promotes stacking fault formation and facilitates the stress-induced transformation from the face centered cubic (FCC) to hexagonal close-packed (HCP) structure. HEAs with higher Mn content, such as CrMnFeCoNi, typically exhibit pronounced TRIP behavior at both cryogenic and ambient temperatures. However, excessive Mn addition may lead to elemental segregation or compromise chemical homogeneity [59].

Cobalt (Co) also contributes to lowering the SFE and enhances twinning activity, particularly in combination with Mn. It strengthens the solid solution and helps retain ductility in systems Chromium (Cr), widely known for its corrosion resistance, stabilizes the FCC phase but can promote the formation of body centered cubic (BCC) phases or even brittle intermetallics such as the σ-phase when added in higher concentrations. Cr-rich HEAs often develop dual-phase FCC+BCC microstructures, which promote heterogeneous deformation and improve work-hardening behavior [60].

Nickel (Ni) serves as an FCC stabilizer and increases the SFE, thereby suppressing both twinning and phase transformations. While Ni enhances ductility and thermal stability, it can diminish TRIP activity. Reducing Ni content in alloys such as CrMnFeCoNi resulting in compositions like CrMnFeCo has been shown to increase TRIP effectiveness due to the corresponding drop in SFE [61].

Iron (Fe), although relatively neutral in its effect on SFE, plays an important supporting role. It contributes to the mechanical and chemical balance of multicomponent systems through solid solution strengthening and supports the integrity of the FCC phase structure [20].

Other elements such as aluminum (Al), titanium (Ti), niobium (Nb), and various refractory metals also have critical effects. Al tends to raise SFE and promote the formation of BCC or ordered B2 phases, increasing strength but often reducing ductility particularly in dual-phase FCC+BCC structures [62]. Ti and Nb tend to induce intermetallic phase formation, which may enhance strength at elevated temperatures but reduce ductility at room temperature [63]. Refractory elements like molybdenum (Mo), tungsten (W), and tantalum (Ta), commonly found in refractory HEAs (RHEAs), offer exceptional high-temperature performance and oxidation resistance, although their inclusion often leads to brittleness at lower temperatures [56]. The influence of individual alloying elements on SFE, FCC stability, and TRIP tendency is summarized in Figure 2.7.

Figure 2.7: *Qualitative effect of key alloying elements on stacking fault energy (SFE), FCC phase stability, and TRIP tendency in FCC-based HEAs. Negative SFE values indicate a reduction that promotes TRIP, while positive values suggest suppression. Phase stability reflects FCC retention, and TRIP tendency shows each element's influence on transformation-induced plasticity.*

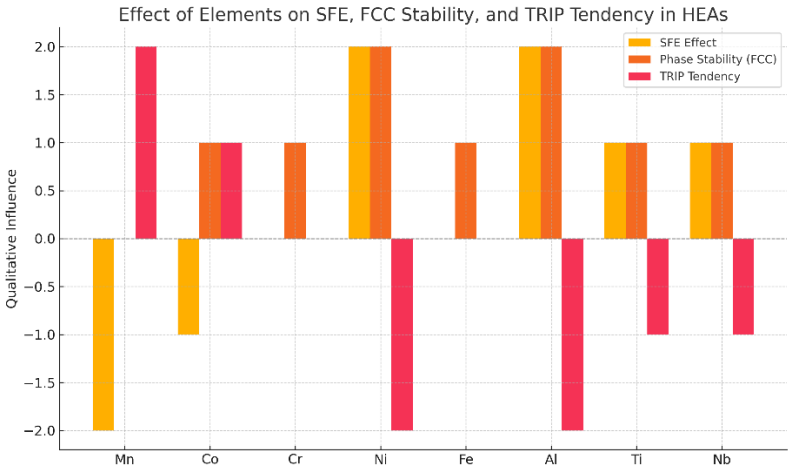

2.4.2 Non-Equiatomic HEAs and Tailored TRIP Behavior

While equiatomic high-entropy alloys (HEAs) such as CrMnFeCoNi have played a foundational role in establishing our understanding of mechanical behavior in complex alloys, recent developments have shifted attention toward non equiatomic compositions. These alloys offer significantly more flexibility in compositional design, enabling precise control over phase stability, stacking fault energy (SFE), and deformation mechanisms particularly transformation induced plasticity (TRIP). By moving beyond the equal atomic percentage constraint, researchers can optimize the balance between strength, ductility, and thermal stability for specific applications [64,65]. Adjusting the elemental ratios in non-equiatomic high-entropy alloys (HEAs) provides a powerful strategy for fine-tuning the stacking fault energy (SFE), which in turn governs the dominant deformation mechanisms. For example, reducing the nickel (Ni) content in CrMnFeCoNi-

based alloys results in a lower SFE, promoting the transformation from face-centered cubic (FCC) to hexagonal close-packed (HCP) structures and enhancing TRIP activity at both room and cryogenic temperatures [66]. Increasing the manganese (Mn) content further decreases SFE, thereby encouraging mechanical twinning and stress-induced martensitic transformation [67]. In parallel, adjusting cobalt (Co) or iron (Fe) levels can help suppress the formation of undesirable intermetallic phases and improve the alloy's work-hardening behavior [68]. A prominent example of such compositional tuning is the non-equiatomic alloy $Cr_{20}Mn_{30}Fe_{20}Co_{20}Ni_{10}$, which demonstrates excellent strain hardening and mechanical strength. This performance is attributed to its optimized SFE, estimated at around 13–15 mJ/m², which supports stable TRIP behavior at room temperature [5]. Similarly, the composition $Cr_{26}Mn_{30}Fe_{20}Co_{15}Ni_{9}$ undergoes a dual-phase transformation (FCC+HCP) during deformation, enabling progressive phase transformation and maintaining high ductility throughout plastic deformation [65].

Such non-equiatomic designs offer multiple advantages, including the activation of TRIP at lower applied strains, the extension of strain hardening over prolonged deformation, and the retention of high ductility even at elevated strength levels. Their compositional flexibility also makes them ideal candidates for temperature-targeted mechanical design. In cryogenic environments, reducing Ni while increasing Mn or Co concentrations has been shown to lower SFE and intensify TRIP activity at −196 °C [69]. For intermediate temperature applications (200–400 °C), minor additions of elements like aluminum (Al) or silicon (Si) can maintain phase transformation capability while simultaneously enhancing oxidation resistance [70]. At elevated temperatures, elements such as Al and titanium (Ti) contribute to the stabilization of the BCC phase and encourage precipitate formation, which improves creep resistance and overall thermal

stability [55]. In particular, dual-phase non-equiatomic systems such as $Al_{0.5}CrCoFeMnNi$ incorporate both FCC and BCC phases, introducing mechanical heterogeneity that enhances strength through interfacial hardening and transformation-assisted plasticity an effective strategy for components under complex loading conditions [71].

2.5 Grain Structure and Dual Phase Formation

The mechanical behavior of HEAs, particularly their capacity for transformation-induced plasticity (TRIP), is governed not only by composition but also by the material's microstructural architecture especially the grain structure and phase distribution. Recent studies have shown that designing heterogeneous microstructures, including dual-phase systems such as FCC + BCC or FCC + HCP, provides a powerful means to optimize the often-conflicting requirements of strength, ductility, and work hardening in TRIP assisted HEAs [72–74] . Grain size and morphology significantly influence deformation behavior. Ultrafine and nanocrystalline grains generally lead to higher strength due to the Hall–Petch effect but may reduce ductility and suppress TRIP activity by limiting the transformation volume and the development of stacking faults [25]. In contrast, heterogeneous grain structures composed of both coarse and fine grains promote strain-gradient plasticity. In such systems, the softer (coarse-grained) regions accommodate plastic deformation, while the harder (fine-grained) regions accumulate geometrically necessary dislocations (GNDs), which serve as nucleation sites for twinning and martensitic transformation [75]. Coarse grains are particularly effective in sustaining TRIP and mechanical twinning, thereby contributing significantly to elongation, while fine grains reinforce the material's strength.

Controlled thermomechanical processing, such as cold rolling followed by annealing, has been employed to create dual-scale grain structures that combine these effects [76]. This strategy enables a synergy between strength and ductility that surpasses what is typically achievable in homogeneous microstructures. Dual-phase architectures in HEAs can either be static formed during solidification or post-processing or dynamic, evolving during deformation as stress-induced phase transformations (e.g., FCC → HCP) occur [77]. In both cases, the introduction of phase boundaries plays a critical role. These interfaces act as dislocation barriers, enhance strain partitioning, and delay the onset of necking by sustaining high work-hardening rates. Examples of such systems include $Al_{0.3}CoCrFeNi$, which exhibits a stable dual-phase FCC + BCC microstructure. In this alloy, dislocations pile up at phase boundaries, significantly enhancing strength without severely compromising ductility. Another notable case is CrCoNi, where deformation induces the formation of HCP nano-lamellae within FCC grains. This dynamic dual-phase structure improves both strength and ductility by enabling progressive transformation while maintaining high structural integrity [48].

Overall, microstructural design especially through the introduction of grain and phase heterogeneity plays a crucial role in activating and sustaining TRIP in HEAs. These effects can often exceed the impact of composition alone, underscoring the importance of integrating processing strategies into alloy design.

2.6 Stacking Fault Energy and Its Role in Deformation Mechanisms of FCC Based HEAs

Stacking fault energy (SFE) is a critical thermodynamic parameter that governs the deformation behavior of face-centered cubic (FCC) high-entropy alloys (HEAs). It represents the energy cost per unit area to form a stacking fault a planar defect caused by a local disruption in the ideal atomic stacking sequence (e.g., ABCABC → ABCABABC), resulting in regions with hexagonal close packed (HCP) like character [78,79]. Mathematically, SFE can be approximated by the expression:

$$\gamma\text{SFE} = \frac{\Delta G^{\gamma\to\varepsilon}}{a\,.\,N_A} \tag{2.7}$$

In this context, $\Delta G^{\gamma\to\varepsilon}$ represents the Gibbs free energy difference between the face-centered cubic (FCC, γ) and hexagonal close-packed (HCP, ε) phases, a denotes the interplanar spacing, and N_A is Avogadro's number. The stacking fault energy (SFE) is directly influenced by both temperature and alloy composition. Elements that stabilize the FCC phase, such as nickel (Ni), tend to increase SFE, whereas elements like manganese (Mn) and cobalt (Co), which either stabilize the HCP phase or destabilize FCC, contribute to a reduction in SFE. This thermodynamic relationship is often expressed using the following formulation:

$$\gamma\text{SFE} \propto \Delta G^{\gamma\to\varepsilon} = G_{HCP} - G_{FCC} \tag{2.8}$$

Shows that this energy difference, and hence SFE, is temperature dependent. At lower temperatures, reduced entropy contributions typically lower SFE, favoring mechanisms like TRIP and TWIP [80,81]. The stacking fault energy (SFE) serves as a

critical parameter in determining the dominant deformation mechanisms in FCC-based high-entropy alloys (HEAs). Based on its value, three principal regimes can be defined. In the low SFE regime (less than 20 mJ/m²), stacking fault formation and deformation-induced martensitic transformation from FCC to HCP structures are favored, thereby activating transformation-induced plasticity (TRIP). Alloys such as CrCoNi and nickel-lean variants of CrMnFeCoNi typically fall within this category. In the intermediate SFE range (20–45 mJ/m²), mechanical twinning becomes the dominant deformation mode, known as twinning-induced plasticity (TWIP). A representative example is the equiatomic CrMnFeCoNi alloy, which typically has an SFE between 22 and 30 mJ/m² and exhibits pronounced twinning during the early stages of deformation, contributing significantly to work hardening. In contrast, the high SFE regime (greater than 45 mJ/m²) favors dislocation slip as the primary deformation mechanism while suppressing both TRIP and TWIP. This behavior is commonly observed in HEAs with high nickel content or those alloyed with aluminum. As shown in Table Compositional tuning is a powerful strategy to manipulate SFE and optimize deformation behavior:

Table 2.4: *Influence of composition on stacking fault energy (SFE) and dominant deformation mechanisms in FCC-based high-entropy alloys at room and cryogenic temperatures* [82,83].

Composition	SFE (mJ/m²)	Dominant Mechanism
$Cr_{20}Mn_{30}Fe_{20}Co_{20}Ni_{10}$	~13	TRIP at RT and cryogenic temperatures
CrMnFeCoNi	~22–30	TWIP with some TRIP
CrMnFeCoNi + 5 at.% Al	>45	Dislocation slip; TRIP suppressed

2.7 Lattice Distortion and Atomic Size Mismatch in High Entropy Alloys

In HEAs, lattice distortion is a central microstructural feature resulting from the presence of multiple principal elements with differing atomic radii. This atomic size mismatch leads to a locally irregular crystal structure that significantly impacts both mechanical behavior and phase stability. Far from being a minor side effect, lattice distortion is a deliberately harnessed property in HEA design, offering unique pathways for strengthening and tuning phase transformation behavior [64,84–86]. One of the most widely used metrics to quantify lattice distortion is the δ (delta) parameter, which estimates the degree of atomic size mismatch in a multicomponent system. It is calculated using:

$$\delta = \sqrt{\sum_{i=1}^{n} c_i\left(1 - \frac{r_i}{\bar{r}}\right)} \times 100 \tag{2.9}$$

In this expression, c_i denotes the atomic fraction of the i^{th} element, r_i is the atomic radius of the i^{th} element, and the average atomic radius of the alloy, $\bar{r}$, is calculated as $\bar{r} = \sum c_i r_i$. The atomic size mismatch parameter, often represented by δ, reflects the degree of lattice distortion in the alloy. A higher δ value indicates greater local lattice strain, which can impede dislocation motion and thereby enhance solid solution strengthening. This leads to several mechanical consequences: it increases the yield strength by obstructing slip, suppresses dynamic recovery to preserve strain hardening behavior, and in some cases, may reduce ductility if the distortion becomes excessive or induces phase instability. For instance, the base FCC alloy CrMnFeCoNi has a δ of ~3.8%, while CrCoNi is around ~2.7%. Adding larger atoms like Al or Ti increases δ

(e.g., $Al_{0.3}CoCrFeNi$ has ~5.1%), which raises strength but often destabilizes the FCC matrix, resulting in the formation of BCC phases or dual-phase microstructures [81,86].

The strengthening mechanism associated with distortion is commonly expressed as:

$$\tau_{ss} \propto G \,.\, \epsilon \,.\, c^{\frac{1}{2}} \tag{2.10}$$

In this formulation, τ_{ss} represents the solid solution strengthening stress, G is the shear modulus, ϵ denotes the atomic misfit strain, and ccc is the atomic concentration of solute elements. This relationship highlights how atomic size mismatch quantified by the misfit strain directly contributes to strengthening by increasing resistance to dislocation movement. As solute atoms distort the surrounding lattice, they create local stress fields that interact with dislocations, thereby impeding their motion and enhancing the alloy's mechanical strength. However, lattice distortion also affects phase stability. When the stored elastic strain energy from distortion surpasses the entropy-driven mixing benefit, the alloy may undergo phase separation. This can result in the precipitation of ordered intermetallics (e.g., B2, σ-phase) or a shift from FCC to BCC structures. In Al and Ti containing HEAs, such distortion-induced transitions are well documented. For example, increasing Al content in CoCrFeNi alloys often triggers a transition from a single-phase FCC structure to a dual-phase FCC + BCC microstructure [87,88].

These phenomena are confirmed through both experimental techniques and computational modeling. X-ray diffraction (XRD) patterns show peak broadening in distorted HEAs due to microstrain. This is often analyzed using Williamson–Hall plots to separate strain and crystallite size contributions [89]:

$$\beta \cos \theta = \frac{k\lambda}{D} + 4\epsilon \sin \theta \quad (2.11)$$

In this equation, β represents the peak broadening in radians, θ is the Bragg angle, D denotes the crystallite size, and ϵ corresponds to the lattice strain. These parameters are typically used in X-ray diffraction analysis to evaluate microstructural features such as grain refinement and internal strain. Beyond diffraction-based techniques, high-resolution transmission electron microscopy (HRTEM) provides direct visualization of distorted atomic planes, offering further insight into local lattice strain. Complementary techniques such as atom probe tomography (APT) and energy-dispersive X-ray spectroscopy (EDS) mapping reveal evidence of short-range ordering and elemental clustering, both of which are closely associated with distortion-driven phase behavior in high-entropy alloys.

On the theoretical side, molecular dynamics (MD) simulations demonstrate that distortion creates a rugged potential energy landscape, increasing the stress required for dislocation glide. Density functional theory (DFT) further quantifies changes in lattice parameters, formation energies, and local bond distortions. These calculations reinforce that lattice strain energy is as critical as entropy in stabilizing HEAs. Meanwhile, CALPHAD modeling is increasingly incorporating distortion sensitive parameters to better predict phase formation in systems containing Al, Ti, or Nb [11]. In summary, lattice distortion in HEAs plays a dual role: it enhances mechanical strength by obstructing dislocation motion and modifies phase behavior by destabilizing homogeneous solid solutions under certain conditions. This makes it a powerful design tool but one that must be carefully balanced to avoid sacrificing ductility or phase stability. Through experimental validation and computational insights, lattice distortion

has emerged not as a secondary phenomenon, but as a central principle in the modern design of high-performance HEAs [90].

2.8 GNDs, TRIP Activation, and Summary of Literature Insights

The mechanical performance of high-entropy alloys (HEAs), particularly those with FCC-based or dual-phase structures, is governed by a complex interplay of dislocation mechanisms, phase stability, and microstructural features. Among these, geometrically necessary dislocations (GNDs) play a pivotal role not just in accommodating strain gradients, but in actively promoting transformation-induced plasticity (TRIP) and enhancing strain hardening. The understanding of GNDs and their influence connects directly to broader findings across the HEA literature, including the role of stacking fault energy (SFE), lattice distortion, and thermomechanical conditions. This section outlines the role of GNDs and integrates key findings from prior studies to highlight remaining research gaps [91,92]. In FCC-based HEAs that undergo strain-induced phase transformation (e.g., FCC → HCP), GNDs serve as mechanical hotspots that trigger the onset of TRIP. Localized stress concentrations and plastic strain incompatibilities near grain boundaries, phase interfaces, or heterogeneities create conditions favorable for stacking fault accumulation. These stacking faults act as nucleation sites for HCP lamellae, effectively lowering the energy barrier for transformation [6,93].

Experimental observations using Electron Backscatter Diffraction (EBSD) and Transmission Electron Microscopy (TEM) have shown that regions where HCP nucleates in alloys like CrMnFeCoNi and CrCoNi frequently correspond to areas with high misorientation an indirect signature of elevated GND density. This makes GNDs not

passive carriers of plasticity, but active agents that initiate and sustain phase transformation, particularly under cryogenic conditions where SFE is reduced [94,95]. Beyond TRIP activation, GNDs contribute significantly to the strain hardening response in HEAs. In heterogeneous or dual-phase microstructures, mechanical incompatibility between soft and hard regions causes an accumulation of GNDs, especially at phase boundaries or lamellar interfaces. These dislocations interact with statistically stored dislocations (SSDs), impeding further dislocation motion and increasing flow stress. The strain hardening effect from GNDs can be captured by a modified Taylor hardening model[96,97]:

$$\sigma = \sigma_0 + M + \alpha \cdot \mathrm{G} \cdot \mathrm{b}. \sqrt{\rho\mathrm{SSD} + \rho\mathrm{GND}} \tag{2.12}$$

In this equation, σ denotes the flow stress, while ρSSD and ρGND represent the densities of statistically stored dislocations and geometrically necessary dislocations, respectively. The parameters $\mathrm{M}, \alpha, \mathrm{G}, \mathrm{b}$ correspond to the Taylor factor, a material constant, the shear modulus, and the magnitude of the Burgers vector, respectively. This formulation reflects how dislocation density both from homogeneous storage and from strain gradients directly contributes to the overall flow stress of the material, emphasizing the fundamental role of dislocation interactions in strain hardening. This formulation shows how increasing GND density amplifies strain hardening, helping to maintain strength and ductility over prolonged plastic deformation. Such behavior is especially beneficial in gradient-structured or lamellar HEAs, where alternating microstructural zones accumulate strain at different rates, requiring GND-mediated compatibility [98].

2.9 Summary of Literature Findings and Research Gaps

HEAs have drawn significant attention in recent years due to their remarkable ability to combine strength, ductility, and fracture resistance—particularly at low temperatures. Foundational studies have firmly established that the unique chemistry of HEAs, characterized by multiple principal elements, gives rise to exceptional mechanical behavior. Central to this performance is the activation of deformation mechanisms such as transformation-induced plasticity (TRIP) and twinning-induced plasticity (TWIP), both of which enhance strain hardening and delay failure. While substantial progress has been made, critical questions remain regarding how to precisely control the interplay between composition, microstructure, and deformation pathways. This section consolidates key insights from the literature and identifies the unresolved challenges that motivate the present work.

2.9.1 Key Insights from Previous Studies

Over the past decade, extensive research has established the mechanical superiority of FCC-based high-entropy alloys (HEAs), particularly those based on the CrMnFeCoNi system. These alloys are recognized for their exceptional ductility, fracture toughness, and thermal stability across a wide temperature range. Importantly, even modest compositional adjustments such as variations in manganese (Mn), aluminum (Al), or nickel (Ni) content can significantly alter phase stability, SFE, and overall mechanical response. Among the primary drivers of this outstanding performance are the deformation mechanisms of transformation-induced plasticity (TRIP) and twinning-induced plasticity (TWIP). These mechanisms play a central role in enhancing work hardening and damage tolerance. Their activation is highly dependent on both alloy composition and testing

temperature. In particular, cryogenic environments tend to lower the SFE, which reduces the energy barrier for phase transformation and thereby intensifies TRIP activity. SFE serves as a critical parameter in determining the dominant deformation mechanism. Alloys with SFE values below 20 mJ/m² generally exhibit TRIP, while those within the intermediate range of 20–45 mJ/m² are prone to TWIP-dominated deformation. For alloys with SFE above 45 mJ/m², conventional dislocation slip tends to dominate. Through careful compositional design, SFE can be tailored to control deformation modes and achieve specific mechanical property targets.

Lattice distortion resulting from atomic size mismatch is another important factor influencing mechanical behavior. This distortion leads to solid-solution strengthening and, in the case of heterogeneous or dual-phase microstructures, promotes the accumulation of geometrically necessary dislocations (GNDs), particularly near grain or phase boundaries. GNDs not only contribute to enhanced strain hardening by obstructing dislocation motion but also act as nucleation sites for phase transformations, especially under low-temperature conditions where TRIP is active. Furthermore, the integration of computational and experimental tools has advanced the field significantly. Predictive models developed using density functional theory (DFT), CALPHAD thermodynamic assessments, and molecular dynamics (MD) simulations have successfully identified trends in phase stability, SFE, and strengthening mechanisms. These models have been validated by experimental techniques such as electron backscatter diffraction (EBSD), transmission electron microscopy (TEM), and X-ray diffraction (XRD), which confirm the presence of HCP lamellae, twinning, and GND clusters in deformed regions of the material. Despite these advancements, several critical gaps remain in the current understanding of HEAs. Firstly, much of the existing research has focused on equiatomic

systems, such as CrMnFeCoNi and CrCoNi, while non-equiatomic compositions particularly those subjected to thermomechanical processing are less well understood. Secondly, while the role of GNDs in enhancing strength is acknowledged, their evolution across a broad temperature spectrum, from cryogenic to elevated conditions, has not been systematically characterized in heterogeneous HEAs.

Another unresolved issue is the lack of a quantitative relationship between lattice distortion and TRIP behavior. Although qualitative correlations between the atomic size mismatch parameter (δ) and transformation activity have been proposed, predictive models that directly link atomic misfit, local distortion energy, and phase transformation remain underdeveloped. Additionally, while the individual effects of processing parameters such as rolling, annealing, and thermal exposure have been studied, their combined influence on deformation mechanisms and microstructure stability has yet to be comprehensively explored. Moreover, there is a shortage of comparative studies evaluating the same alloy across diverse temperature regimes. Such investigations are essential to understanding phase transformation stability, work hardening behavior, and service performance under realistic operating conditions. To address these gaps, the present study investigates a non-equiatomic CrCoNiFeMn high-entropy alloy processed via cold rolling followed by post-deformation annealing. Tensile testing was conducted at −196 °C, 25 °C, and 400 °C to evaluate the deformation behavior under cryogenic, ambient, and elevated temperature conditions. This work places special emphasis on: (i) the evolution of TRIP activity as a function of temperature, (ii) the influence of stacking fault energy on deformation mechanisms, and (iii) the formation and distribution of geometrically necessary dislocations in dual-phase microstructures. By integrating detailed microstructural characterization with mechanical testing across a range of

thermal environments, this study aims to clarify the coupled effects of composition, processing, and temperature on phase transformation behavior and strain hardening in structurally and compositionally complex HEAs.

3. Materials and Methods

3.1 Alloy Design and Fabrication

3.1.1 Selection of Elements and Design Rationale

The alloy explored in this study is a non-equiatomic CrCoNiFeMn based HEA, specifically designed to develop a dual-phase microstructure and exhibit transformation-induced plasticity (TRIP) across a wide temperature range. The composition was carefully tailored by considering the distinct roles of each element in controlling phase stability, stacking fault energy (SFE), and the dominant deformation mechanisms. The base elements Cr, Co, Ni, Fe, and Mn were selected due to their well-established ability to form stable FCC solid solutions known for high ductility and strong work-hardening behavior. Among them, Ni and Co act as FCC phase stabilizers, reducing the driving force for phase transformation and thereby helping to preserve ductility at room and elevated temperatures. On the other hand, Cr and Mn introduce chemical and lattice-level instabilities in the FCC matrix, encouraging FCC to BCC phase transformation under mechanical loading a key trigger for the TRIP effect, particularly at cryogenic temperatures.

Fe plays a dual role by improving both ductility and thermal stability while also contributing to solid solution strengthening. The choice to move away from an equiatomic composition was intentional: this deviation introduces phase metastability and microstructural heterogeneity, which enhance the alloy's ability to store dislocations and promote strain partitioning during deformation. The choice of elements in this alloy was primarily influenced by their impact on stacking fault energy (SFE). Both theoretical

predictions and experimental findings indicate that reducing the SFE to around 15–20 mJ/m² enables stress-induced martensitic transformation from FCC to BCC a key mechanism behind the TRIP effect. In this regard, the inclusion of Cr and Mn plays a crucial role by lowering the SFE, making the alloy more prone to phase transformation under mechanical strain, particularly at cryogenic temperatures. Additionally, adopting a non-equiatomic composition encourages the development of heterogeneous microstructures, often resulting from enhanced elemental segregation during solidification or subsequent thermomechanical processing. This microstructural heterogeneity creates local variations in SFE and strain distribution, which not only promote TRIP activation but also lead to increased accumulation of geometrically necessary dislocations (GNDs). Together, these effects significantly enhance the alloy's strain-hardening response. The estimated stacking fault energy (SFE) for the present alloy at room temperature lies in the range of 33–51 mJ/m^{-2}. Theoretical Calculations for the configurational Entropy of mixing is demonstrated below:

$$\Delta S_{config} = -R \sum_i^n x_i \ln x_i \tag{3.1}$$

Where $R = 8.314462618 \frac{J}{mole.K}$ and x_i are the atomic fractions of the constituent elements. For x = {0.3, 0.3, 0.25, 0.1, 0.05} the summation

$$\sum x_i \ln x_i = -1.4490 \tag{3.2}$$

Therefore,

$$\Delta S_{config} = -R(-1.4490) = 12.05 \frac{J}{mole.K} \tag{3.3}$$

Based on the configurational entropy calculation our composition is placed in between the transition between medium entropy and high entropy cluster [99]. The compositional design of the alloy was informed by insights from both empirical data and thermodynamic modeling, including CALPHAD simulations and ab initio density functional theory (DFT) calculations reported in the literature. These tools were instrumental in predicting phase stability and transformation behavior across a range of temperatures, helping to tailor the alloy's metastability for dynamic phase changes during tensile deformation. This alloy was intentionally selected as a model system to investigate how temperature, microstructure, and composition interact to influence the TRIP effect. Its design reflects a broader shift in high entropy alloy research, where non-equiatomic compositions are increasingly explored to achieve unique property combinations through deliberate chemical tuning.

3.1.2 Alloy Melting, Casting, and Homogenization

The alloy used in this study was produced using vacuum induction melting (VIM), a well-established method for fabricating high-purity HEAs. This technique is particularly suitable for multicomponent systems, as it minimizes contamination an important consideration given that even trace impurities can impact phase stability, grain structure, and stacking fault energy (SFE). The target composition was $Fe_{30}Cr_{30}Ni_{25}Mn_{10}Co_5$ (at%), a non-equiatomic derivative of the Cantor alloy, deliberately designed to promote microstructural heterogeneity and deformation-induced phase transformations [100]. High-purity elemental feedstock materials (Cr, Co, Ni, Fe, and Mn, each with purity above 99.9%) were carefully weighed according to the intended atomic ratios and melted in an alumina crucible under a protective argon atmosphere. This inert environment

helped prevent oxidation and reduce volatilization losses especially important for manganese, given its relatively high vapor pressure. The melt was held at 1650–1700 °C for 10–15 minutes to ensure full dissolution of the elements and achieve chemical homogeneity. After homogenization, the alloy was cast into a water-cooled copper mold, promoting rapid solidification. This step was crucial for minimizing elemental segregation and avoiding dendritic growth, which can otherwise introduce microstructural anisotropy in as-cast HEAs. The resulting ingot, approximately 100 mm long and 20 mm in diameter, provided a convenient form for further thermomechanical processing, including homogenization, cold rolling, and heat treatment.

Post-solidification, the alloy was subjected to a homogenization heat treatment at 1150 °C for 12 hours in vacuum, followed by water quenching. This step was designed to eliminate residual elemental segregation caused by non-equilibrium solidification and to stabilize a single-phase FCC matrix before cold rolling. Literature reports indicate that homogenization at such elevated temperatures effectively dissolves interdendritic precipitates and reduces microsegregation in CrMnFeCoNi-based HEAs. X-ray diffraction (XRD) and backscattered electron (BSE) imaging confirmed the formation of a single-phase FCC structure in the homogenized condition with uniform elemental distribution and no evidence of second-phase precipitates. This phase purity was crucial to isolate the effect of thermomechanical processing and heat treatment on the development of dual-phase microstructures and TRIP activation in later stages [40]. To ensure repeatability and maintain compositional consistency, two ingots were independently fabricated using the same processing parameters. Energy-dispersive X-ray spectroscopy (EDS) was performed on multiple regions of each ingot, revealing only minor deviations ess than 1 at.% from the intended composition. These results confirmed

the reliability and reproducibility of the melting and casting procedure, providing a solid foundation for subsequent mechanical testing and microstructural analysis.

3.2 Thermomechanical Processing

3.2.1 Cold Rolling Procedure

After homogenization, the alloy ingots were machined into rectangular sheets measuring approximately 60 mm × 10 mm × 5 mm and then cold rolled to introduce plastic deformation, refine the microstructure, and promote phase metastability key conditions for activating the TRIP effect. Cold rolling was carried out at room temperature using a two-high laboratory rolling mill, with the rolling direction aligned along the sample's longitudinal axis. The rolling process was performed in multiple passes, with thickness reductions of 5-10% per pass, until an overall reduction of about 80% was reached. Lubrication was applied throughout to reduce friction and prevent surface cracking, particularly in the final stages. No intermediate annealing was performed between passes to retain deformation-induced defects and stored energy, both of which are essential for subsequent microstructural evolution during post-rolling heat treatment. This cold working process generated a high dislocation density and introduced significant microstructural heterogeneity, including deformation bands and shear zones. These features contribute to local strain incompatibility during tensile loading, enhancing the accumulation of geometrically necessary dislocations (GNDs) and creating favorable conditions for BCC phase nucleation both of which increase the likelihood and extent of TRIP activation.

3.2.2 Post Deformation Annealing Treatments

Following cold rolling, the deformed samples underwent annealing to trigger microstructural recovery, partial recrystallization, and dual-phase formation all critical to enhancing the TRIP effect during subsequent tensile deformation. The annealing process was carefully optimized to preserve elements of the deformed structure while initiating the heterogeneous nucleation of secondary phases, such as BCC or HCP, depending on local compositional and strain conditions. The cold-rolled specimens were annealed at 750 °C for 30 minutes in a vacuum furnace, followed immediately by water quenching. This temperature was selected based on previous studies indicating that intermediate annealing temperatures (600–800 °C) in CrMnFeCoNi-based HEAs promote partial recrystallization while maintaining stored deformation energy and substructural features. Rapid quenching was employed to lock in the high-temperature microstructure and prevent undesirable grain growth or equilibrium phase formation during cooling.

The annealing treatment applied in this study resulted in the development of a heterogeneous dual-phase microstructure. This structure consisted of recrystallized face centered cubic (FCC) grains characterized by a reduced dislocation density, alongside retained deformed FCC regions that remained enriched with dislocation substructures. In addition, discrete body-centered cubic (BCC) phase precipitates were observed, frequently forming along grain boundaries and within shear bands sites typically associated with local stress concentration and plastic instability. Microstructural analysis performed using scanning electron microscopy (SEM) and electron backscatter diffraction (EBSD) revealed several important features following annealing at 750 °C. The recrystallized regions exhibited refined grains with an average grain size of

approximately 850 nm. A notable increase in the fraction of low-angle grain boundaries was also detected, suggesting the occurrence of subgrain recovery and partial restoration processes. Furthermore, the formation of a secondary BCC phase was identified, comprising roughly 6% of the microstructure. These BCC regions were predominantly located at microstructurally stressed zones, such as phase interfaces and deformation bands. Their distribution and morphology play a crucial role in enabling transformation-induced plasticity (TRIP) during mechanical loading, as visually demonstrated in Figure 3.2. X-ray diffraction (XRD) confirmed the coexistence of FCC and BCC phases, with distinct but minor peaks corresponding to the BCC component (See Figure 3.2). The resulting dual-phase architecture fosters strain partitioning during loading, increases dislocation storage capacity, and supports stress-assisted phase transformation, particularly under cryogenic and room-temperature conditions thus amplifying the alloy's TRIP response.

3.3 Microstructural Characterization

3.3.1 Pre and Post Tensile Test Analysis via XRD and EBSD

To investigate the microstructural and phase evolution resulting from thermomechanical processing and subsequent tensile deformation, X-ray diffraction (XRD) and electron backscatter diffraction (EBSD) analyses were performed on both the pre-tensile (as-annealed) and post-tensile (deformed) samples. These complementary techniques offered valuable insights into phase composition, grain orientation, strain accommodation, and deformation induced transformations particularly the stress-assisted FCC to BCC phase transition, which is central to the TRIP effect observed in this dual-phase high-entropy alloy. XRD measurements were carried out using Cu Kα radiation

over a 2θ range of 20° to 100°, with a step size of 0.01° and a dwell time of 0.1 seconds per step. Prior to analysis, all samples were mechanically polished to achieve a flat, reflective surface suitable for accurate diffraction (See Figure 3.2 and Figure 3.3).

In the pre-tensile (as-annealed) condition, diffraction patterns showed prominent peaks corresponding to the FCC phase, with minor contributions from the BCC phase already present in the microstructure. After tensile deformation, particularly in samples tested at −196 °C and 25 °C, a noticeable increase in the intensity of BCC peaks was observed, indicating a stress- or strain-induced transformation from FCC to BCC a key signature of the TRIP effect. Additionally, peak broadening was evident in both cold-rolled and post-deformed specimens, which is attributed to high dislocation densities and lattice distortion. The degree of broadening correlated with the extent of plastic deformation and test temperature, with the cryogenically tested samples exhibiting the most pronounced features.

EBSD characterization was performed on both pre and post tensile samples using a field-emission scanning electron microscope (FE-SEM) equipped with an EBSD detector. Surface preparation included mechanical polishing followed by final finishing with colloidal silica to produce a deformation-free surface ideal for high-resolution orientation mapping (See Figure 3.2, Figure 3.3, and Figure 3.4). In the as-annealed samples, EBSD maps revealed a heterogeneous microstructure composed of recrystallized FCC grains interspersed with deformed subgrains. Kernel Average Misorientation (KAM) analysis indicated moderate local misorientation, consistent with residual strain from prior cold working and partial recrystallization. After tensile testing, KAM values increased significantly particularly near grain boundaries and triple junctions indicating the accumulation of geometrically necessary dislocations (GNDs) as

a result of plastic strain. Samples tested at cryogenic temperatures exhibited clear signs of strain localization and phase transformation, often aligned with shear bands and regions of elevated plastic deformation. Phase maps derived from EBSD indexing confirmed the progressive emergence of the BCC phase in the deformed state. These findings support the mechanism of localized stress-assisted phase transformation, consistent with the activation of the TRIP effect driven by mechanical instability and lattice distortion.

3.4 Mechanical Testing

3.4.1 Tensile Testing Setup and Parameters

Tensile specimens were fabricated in a miniature dog-bone geometry with gauge dimensions of approximately 15 mm in length, 3 mm in width, and 1.4 mm in thickness. This geometry conforms to standard practices for thin-sheet materials and was selected to ensure reliable mechanical testing within the limits of available sample size. All specimens were precisely cut using wire electrical discharge machining (EDM) to minimize edge damage and thermal effects. To achieve a uniform surface finish, the samples were sequentially ground with silicon carbide (SiC) abrasive papers up to 1200 grit and then polished to a mirror finish. Uniaxial tensile tests were conducted using an Instron servo hydraulic mechanical testing machine at three distinct temperatures: cryogenic (−196 °C), ambient (25 °C), and elevated (+400 °C). A constant engineering strain rate of 10^{-3} s^{-1} was applied for all tests. This temperature range was selected to explore the effect of thermal activation on deformation behavior and to assess the contribution of transformation-induced plasticity (TRIP). Consistent sample preparation and test protocols ensured high reproducibility and minimized external influences on fracture behavior, strain localization, and work-hardening characteristics.

3.4.2 Mechanical Behavior at Cryogenic, Room, and Elevated Temperatures

To assess the influence of temperature on mechanical performance and active deformation mechanisms, the tensile behavior of the dual-phase TRIP-assisted high-entropy alloy was systematically investigated at −196 °C (cryogenic), 25 °C (room temperature), and 400 °C (elevated temperature). The results revealed substantial temperature-dependent variations in strength, ductility, and the degree of TRIP activation, as illustrated in Figure 3.1. At -196 °C, the annealed alloy exhibited exceptional mechanical performance, with an ultimate tensile strength (UTS) of approximately 1600 MPa and a uniform elongation approaching 18%. This combination of strength and ductility surpasses the typical strength–ductility trade-off observed in conventional alloys and underscores the dominant role of transformation-induced plasticity at cryogenic temperatures. Several factors contributed to this behavior, including the reduction in stacking fault energy (SFE), which facilitated stress-assisted transformation from the FCC to the BCC phase. Post-mortem EBSD analysis confirmed increased dislocation storage and the accumulation of geometrically necessary dislocations (GNDs). Additionally, strain was effectively partitioned between the softer FCC matrix and the harder, transformed BCC regions, which helped delay necking and promoted uniform plastic deformation. These observations are consistent with earlier studies on TRIP-enabled HEAs, where low-temperature metastability and reduced SFE enhance phase transformation and mechanical robustness.

At room temperature (25 °C), the alloy continued to display a desirable balance between strength and ductility. The UTS ranged from 1050 to 1100 MPa, accompanied by a total elongation of around 10%. Although the extent of FCC to BCC transformation was reduced compared to cryogenic conditions, EBSD phase mapping still revealed

localized TRIP activity, particularly along shear bands and at grain boundary intersections. The operative deformation mechanisms at this temperature included dislocation glide within the FCC matrix, localized hardening due to TRIP in the dual-phase regions, and GND formation near grain boundaries to accommodate strain. While the TRIP effect was not as pronounced as at −196 °C, its continued presence confirmed that the alloy retained sufficient metastability at room temperature to influence deformation behavior.

At 400 °C, mechanical performance declined, with UTS values decreasing to approximately 850 MPa and total elongation falling to about 8%. This reduction in performance is primarily attributed to the activation of thermally driven mechanisms such as dislocation climb and dynamic recovery, which lower the work-hardening rate and flow stress. The TRIP effect was largely suppressed at this temperature due to elevated SFE, which stabilized the FCC phase and reduced the driving force for martensitic transformation. As a result, phase instability was minimized, and strain-induced phase transformation was either limited or absent. Furthermore, thermal softening and increased dislocation mobility led to lower work-hardening rates. Despite these reductions in strength and ductility, the alloy maintained structural integrity and thermal stability, indicating its potential for application in elevated-temperature environments where TRIP activation is not essential.

4. Results and Discussion

4.1 Mechanical Properties at Varying Temperatures

To investigate the influence of temperature and processing history on the mechanical response of the dual phase TRIP-assisted HEA, uniaxial tensile tests were performed at −196 °C (cryogenic), 25 °C (room temperature), and 400 °C (elevated temperature). Two material states were evaluated: the homogenized condition (as-received) and the annealed condition, which had undergone cold rolling followed by heat treatment. These conditions were selected to highlight the effects of microstructural refinement and stored deformation energy on temperature-dependent deformation behavior. At all testing temperatures, the annealed samples demonstrated higher strength than the homogenized counterparts. This improvement is primarily attributed to the finer microstructure and higher dislocation density introduced by cold working. However, this increased strength came at the expense of ductility, particularly at room and high temperatures, where strain localization occurred more readily. In contrast, the homogenized samples, with their coarser and more stable microstructure, showed superior elongation and a more gradual deformation behavior. The mechanical performance was most favorable at cryogenic temperatures for both conditions. At −196 °C, the material exhibited a pronounced strength–ductility synergy, especially in the annealed state. This enhancement is closely associated with the activation of the transformation-induced plasticity (TRIP) effect. The lower stacking fault energy (SFE) at cryogenic temperatures promotes the stress-assisted martensitic transformation from

face-centered cubic (FCC) to body-centered cubic (BCC), which significantly boosts strain hardening and delays necking.

At room temperature, the TRIP effect was still active but less dominant. The material retained good strength and moderate ductility, with phase transformation occurring primarily in localized deformation bands. The mechanical behavior in this regime was governed by a combination of dislocation glide and transformation-induced hardening, particularly in the annealed samples. In contrast, tensile deformation at 400 °C revealed a distinct change in deformation mode. Here, thermally activated mechanisms such as dynamic recovery and dislocation climb reduced the overall strain hardening capacity. The increased SFE at elevated temperatures stabilized the FCC phase and effectively suppressed the TRIP mechanism. As a result, both strength and ductility decreased, particularly in the annealed condition, which showed signs of early strain localization and softening. The homogenized samples, however, retained moderate ductility due to their coarser grain structure and lower initial dislocation density.

These results demonstrate that temperature plays a critical role in determining the balance between dislocation-mediated plasticity and transformation-induced hardening in this dual-phase HEA system. A detailed overview of true stress–strain curves and corresponding strain hardening rates for both conditions is provided in Figure 3.1.

Figure 3.1: *(a and b) True stress/strain and (c and d) strain hardening rate plots for the as-received (a and c) and annealed (b and d) conditions during tensile testing at -196, +25, and 400°C.*

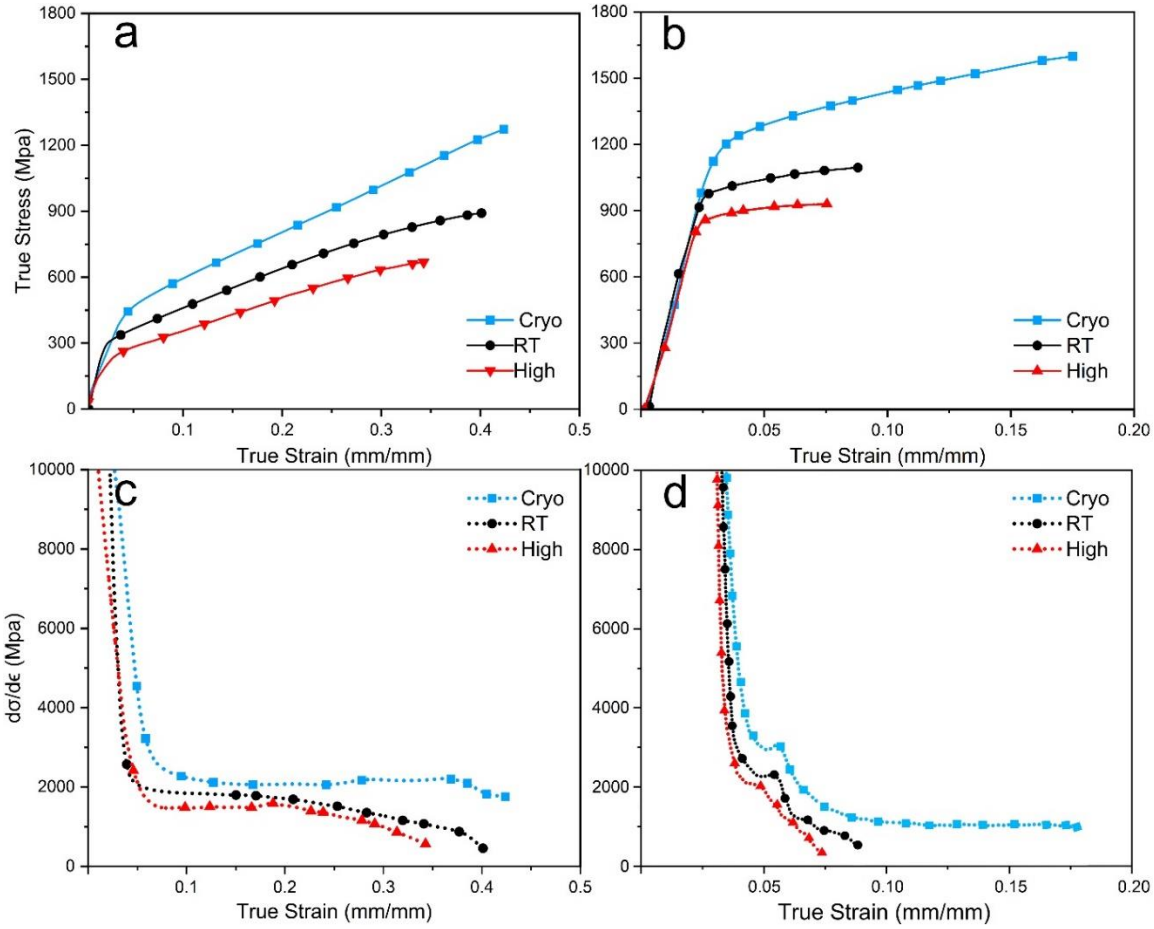

4.2 Phase Transformation Behavior Across Temperatures

The mechanical performance of the dual-phase TRIP-assisted high-entropy alloy (HEA) is intricately linked to its ability to undergo deformation-induced phase transformation. Central to this behavior is the stress- or strain assisted conversion of the metastable face centered cubic (FCC) matrix into a body centered cubic (BCC) phase. This transformation, which underpins the TRIP (transformation-induced plasticity) effect, is highly sensitive to temperature and plays a crucial role in governing the material's

strain-hardening response and strength–ductility synergy. To investigate how this transformation evolves under different thermal conditions, both X-ray diffraction (XRD) and electron backscatter diffraction (EBSD) analyses were performed on samples in the homogenized (as-received) and annealed conditions, before and after tensile deformation at −196 °C, 25 °C, and 400 °C. These complementary techniques provided critical insight into the phase distribution, crystallographic orientation, and extent of transformation in response to mechanical loading at varying temperatures. Table 3.1 illustrates the post-deformation phase transformation fractions of annealed samples tested at cryogenic, room, and elevated temperatures.

Table 3.1: Post deformation phase transformation fractions of annealed samples

Test Temperature	Initial BCC Fraction	Post Deformation BCC Fraction
Cryogenic (-196)	6%	25%
Room (+25)	6%	18%
High (+400)	6%	9%

Figure 3.2: *(a and b) XRD spectra, EBSD results for (c and g) phase maps, (d and h) inverse pole figure (IPF) maps, (e and i) kernel average misorientation (KAM) maps, (f and j) geometrically necessary dislocation (GND) 1012 m-2 maps for the as-received and annealed samples, respectively.*

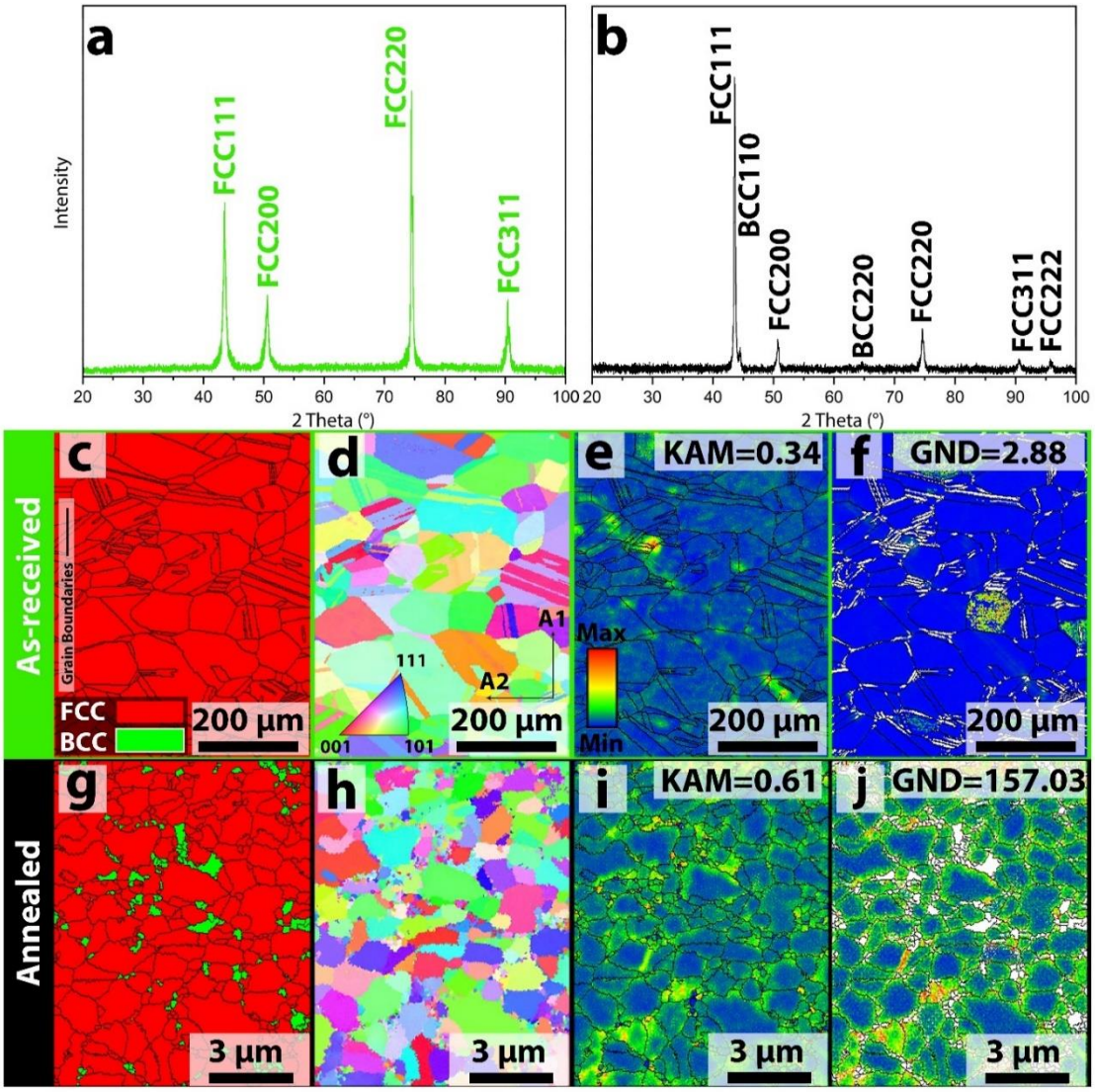

In contrast, the annealed condition displayed clear evidence of temperature-dependent TRIP activity. This condition, obtained through cold rolling followed by annealing at 750 °C for 30 minutes, resulted in a partially recrystallized microstructure with residual strain and substructural heterogeneity. EBSD and XRD analyses of the as-annealed samples revealed a dual-phase configuration comprising approximately 94%

FCC and 6% BCC. The pre-existing BCC phase was distributed along grain boundaries and deformation bands areas typically associated with higher strain localization and transformation potential. This initial metastable microstructure laid the foundation for further transformation under mechanical loading.

At −196 °C, the transformation was most pronounced. Post-deformation XRD spectra showed a significant increase in BCC peak intensities, while EBSD phase maps revealed widespread nucleation of BCC grains throughout the microstructure. These newly formed BCC regions were especially concentrated near grain boundaries, shear bands, and triple junctions microstructural sites where stress and strain localization are highest. The fraction of BCC phase increased markedly from ~6% to approximately 25% after deformation, indicating strong TRIP activation. This transformation played a crucial role in enhancing strain partitioning and delaying necking, which in turn contributed to the superior mechanical properties observed at this temperature.

At 25 °C, the TRIP effect remained active but to a lesser extent. XRD results displayed moderate growth in BCC peaks, and EBSD phase maps confirmed the emergence of new BCC regions, although their distribution was more localized compared to the cryogenic condition. The BCC phase fraction increased to around 18%, highlighting that while transformation still occurred, it was not as widespread. The mechanical response in this regime benefited from the partial transformation, which supported strain hardening and maintained a favorable balance between strength and ductility through localized stress accommodation.

At 400 °C, the transformation was significantly suppressed. Post-deformation characterization showed only a slight increase in BCC content to about 9%, with both XRD and EBSD indicating limited phase evolution. The dominant FCC matrix remained

largely intact, and the microstructure showed signs of thermal recovery and grain coarsening. The increased stacking fault energy (SFE) at elevated temperatures likely stabilized the FCC phase and diminished the driving force required for transformation. As a result, the TRIP mechanism was largely inactive, and the deformation behavior transitioned toward dislocation glide and dynamic recovery, leading to reduced strength and strain hardening capacity.

These observations collectively underscore the strong temperature dependence of phase transformation in this dual-phase HEA. At cryogenic temperatures, reduced SFE and increased lattice instability enhance the FCC-to-BCC transformation, activating the TRIP effect and promoting uniform plastic deformation. At room temperature, partial TRIP activation still contributes meaningfully to strain hardening, albeit at a reduced scale. At elevated temperatures, the transformation is effectively suppressed due to thermally stabilized FCC structure and enhanced recovery mechanisms. This temperature-responsive transformation behavior is consistent with findings reported in the literature. Multiple studies have demonstrated similar trends in metastable HEAs, confirming that TRIP activity is most robust at low temperatures where phase instability and internal stress concentrations favor martensitic transformation [82,101–103]. These results reinforce the idea that controlling phase metastability through processing and alloy design offers a powerful approach to tailoring HEAs for targeted applications, particularly in cryogenic environments where strength–ductility synergy is most critical.

Figure 3.3: XRD spectra after deformation at cryogenic and high temperatures; a) for the as-received sample and b) for the annealed sample.

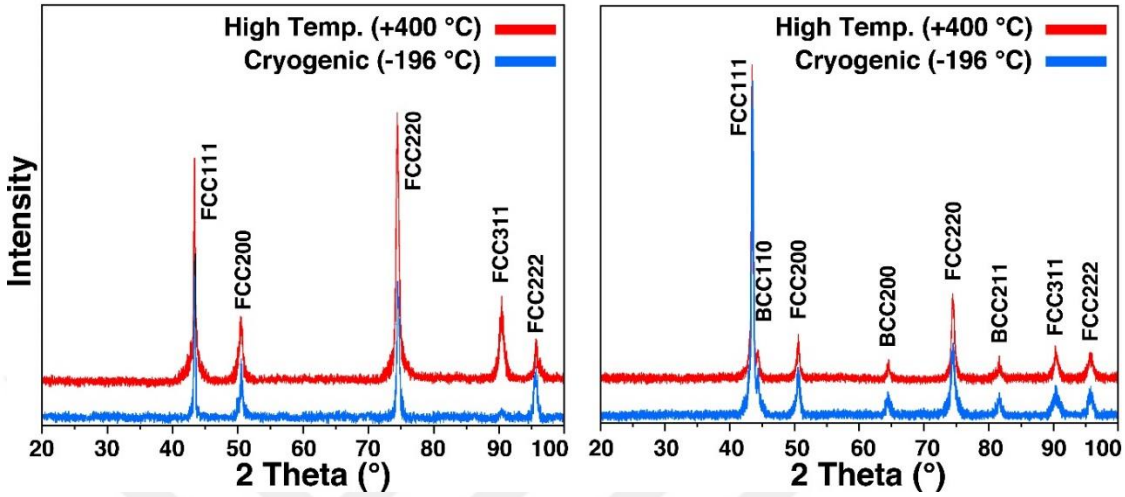

4.3 EBSD Based plastic Deformation and Dislocation Analysis

To better understand the microstructural basis for the observed mechanical behavior, electron backscatter diffraction (EBSD) analysis was employed to assess strain localization and dislocation structures in both the homogenized and annealed conditions across all testing temperatures. Particular attention was given to two key EBSD derived metrics: KAM, which reflects local misorientation due to lattice distortion, and Geometrically Necessary Dislocation (GND) density, which captures dislocations required to accommodate plastic strain gradients. Together, these parameters offer insight into the degree of local plasticity, the nature of hardening mechanisms, and the extent of transformation activity during deformation. EBSD scans were conducted on samples after tensile testing at −196 °C, 25 °C, and 400 °C, with results presented in the form of phase maps, inverse pole Figure 3.4 and Figure 3.5 (IPF) maps, KAM maps, and GND maps. A consistent trend was observed across both microstructural states: as the deformation

temperature decreased, both KAM values and GND densities increased. This trend reflects enhanced dislocation storage and greater internal lattice distortion under lower thermal activation conditions, where recovery and dynamic rearrangement of dislocations are suppressed. The annealed condition exhibited the most pronounced temperature sensitivity in terms of KAM and GND evolution. In the undeformed state, the microstructure already contained moderate levels of misorientation and residual dislocations as a result of prior cold rolling and annealing. After tensile deformation, KAM values showed a clear upward progression with decreasing temperature from ~0.61 in the undeformed state to 0.85, 1.03, and 1.38 following testing at 400 °C, 25 °C, and −196 °C, respectively. This increase in local misorientation highlights intensified strain accumulation at lower temperatures. GND density followed a similar trend, rising from an initial value of ~157×10^{12} m^{-2} in the annealed state to ~257×10^{12} m^{-2} after cryogenic deformation. These high GND levels confirm that plastic strain at low temperatures was accommodated through significant dislocation generation, which is especially notable in regions adjacent to grain boundaries, shear bands, and triple junctions.

Importantly, EBSD phase maps revealed that the spatial distribution of BCC phase formation coincided with regions of high KAM and GND activity. This suggests a strong coupling between stress localization, dislocation pile-up, and transformation-induced hardening a defining characteristic of the TRIP mechanism. At −196 °C, GNDs became more uniformly distributed across the microstructure, extending into grain interiors and larger grains, while at higher temperatures, they remained concentrated in fine grains or localized regions. These findings clearly indicate that the enhanced mechanical performance observed in the annealed condition at low temperatures is not solely due to

phase transformation but also stems from the synergistic interaction between stored dislocations and the evolving dual-phase structure.

Figure 3.4: *EBSD results of the annealed condition for deformation at varying temperatures; (a, e and i) phase maps, (b, f and j) IPF maps, (c, g and k) KAM maps, (d, h and l) GND 1012 m-2 maps.*

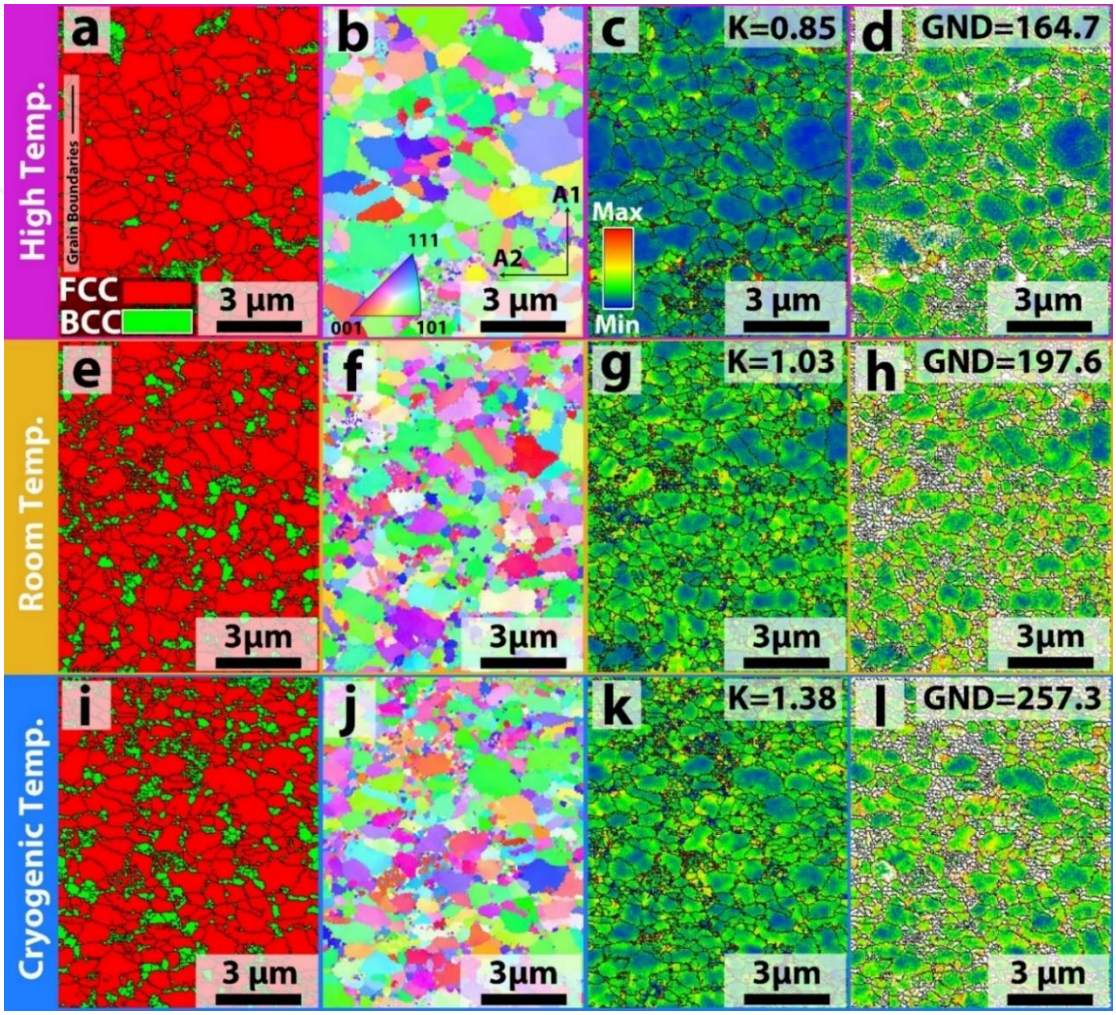

In comparison, the homogenized samples showed more moderate evolution in KAM and GND values with temperature. In the undeformed state, the microstructure was fully recrystallized with equiaxed grains and minimal dislocation content, as confirmed by an initial KAM value of ~0.34 and GND density of ~2.88×10^{12} m^{-2}.

After deformation, KAM increased gradually with decreasing temperature reaching ~2.36 at 400 °C and ~2.66 at −196 °C. While these values reflect strain-induced lattice distortion, the magnitude of change was considerably lower than in the annealed condition. Similarly, GND density increased to approximately 17×10^{12} m^{-2} after deformation but did not vary substantially across different temperatures. This relatively steady GND behavior implies that the misorientation observed in these samples was predominantly due to statistically stored dislocations (SSDs), with limited contribution from GNDs. Furthermore, the absence of any phase transformation in the homogenized condition meant that hardening mechanisms were restricted to dislocation accumulation alone. The lack of microstructural heterogeneity such as phase boundaries or deformation-induced BCC regions reduced the opportunities for back-stress formation and constrained the material's ability to sustain high strain hardening rates, particularly at elevated temperatures.

The EBSD data align well with the mechanical testing results discussed earlier. In the annealed condition, the combination of deformation-induced BCC formation and GND accumulation under low-temperature conditions provided a powerful source of strain hardening, enabling the alloy to achieve gigapascal-level strengths without sacrificing ductility. In contrast, the homogenized condition relied solely on conventional dislocation-mediated hardening and showed less strain partitioning, resulting in lower hardening rates and earlier necking under equivalent loading conditions. Quantitative comparisons of KAM and GND values across temperatures and conditions are presented in Figure 3.4 and Figure 3.5, further illustrating the temperature-sensitive evolution of internal microstructure and its direct impact on deformation behavior.

Figure 3.5: *EBSD results of the as-received condition for deformation at varying temperatures; (a, e, i) phase maps, (b, f, j) IPF maps, (c, g and k) KAM maps, (d, h, l) GND 1012 m-2 maps.*

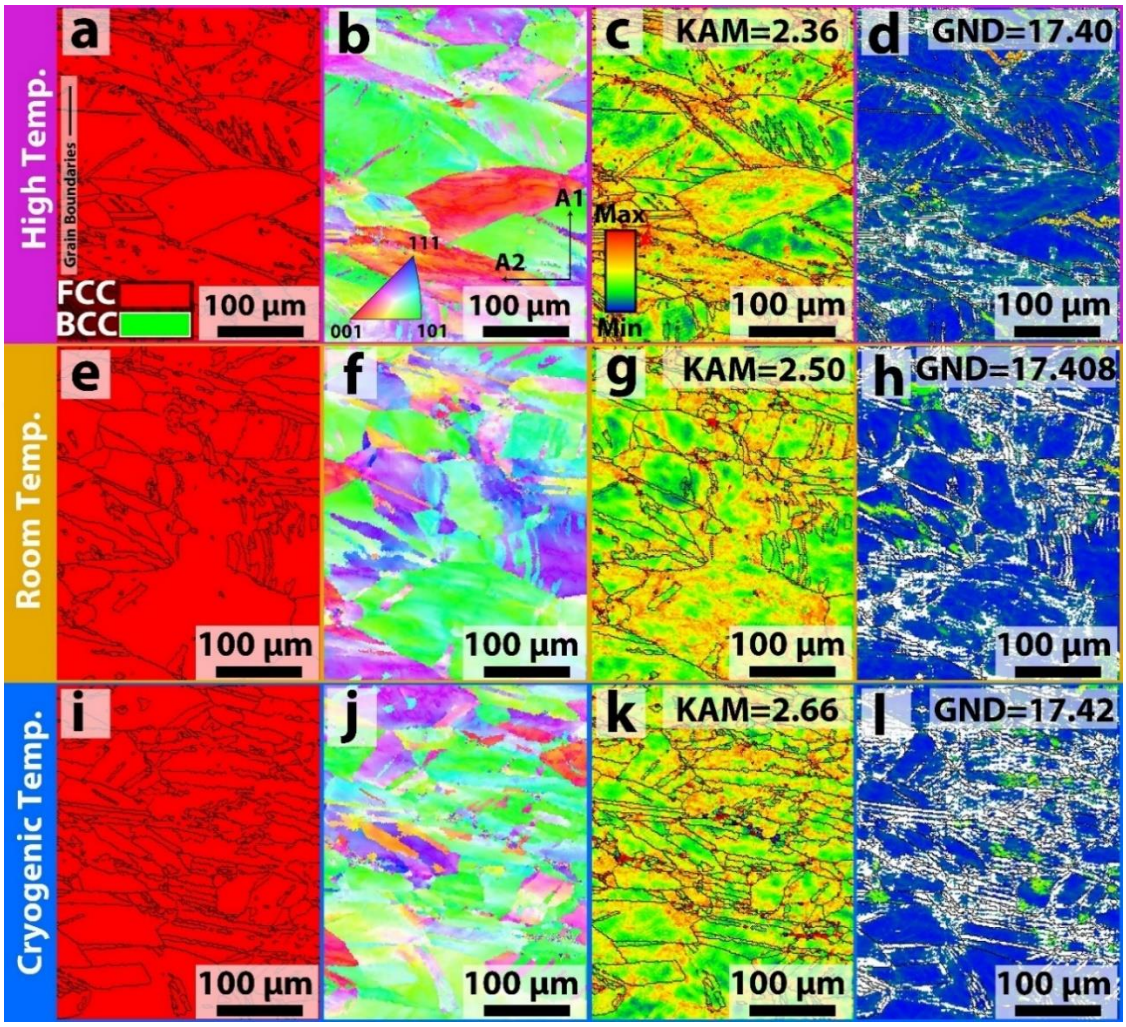

4.4 Discussion on TRIP Activation Mechanisms

The transformation-induced plasticity (TRIP) effect is central to the superior mechanical performance observed in the dual-phase HEA examined in this study. TRIP enhances both strength and ductility by enabling a dynamic phase transformation from a metastable face centered cubic (FCC) matrix to a body centered cubic (BCC) structure during plastic deformation. This mechanism contributes to sustained strain hardening,

delayed onset of necking, and improved energy absorption, particularly under low temperature loading conditions. In this section, the underlying factors governing the activation and extent of the TRIP effect are discussed in light of the experimental findings, with emphasis on phase metastability, stacking fault energy (SFE), chemical composition, microstructure, and deformation temperature. These factors collectively influence the driving force for phase transformation and control the nucleation and growth of the BCC phase during mechanical loading. A key prerequisite for the TRIP effect is the presence of a metastable FCC matrix capable of undergoing stress- or strain-induced transformation. In the annealed condition, the alloy retained a microstructure that was only partially recrystallized following cold rolling and subsequent heat treatment. This structure contained residual dislocation networks and stored strain energy factors that reduce phase stability and increase susceptibility to martensitic transformation.

Pre-deformation EBSD phase analysis confirmed that approximately 6% BCC phase already existed in the annealed samples, likely originating from localized transformation during cold deformation or recovery during annealing. These pre-existing BCC regions were primarily located along grain boundaries and shear bands, acting as nucleation sites for further phase transformation during subsequent mechanical loading. Upon tensile deformation, particularly at −196 °C, these regions expanded and coalesced, increasing the BCC volume fraction and driving the TRIP mechanism forward. In contrast, the homogenized condition, characterized by coarse grains and a fully recrystallized FCC structure, lacked the necessary metastability and internal energy to initiate transformation. As a result, this condition did not exhibit any measurable TRIP behavior across the entire temperature range studied. SFE is a critical material parameter that dictates the prevailing deformation mechanism in FCC systems. High SFE promotes

dislocation glide and climb; intermediate SFE favors mechanical twinning (TWIP); and low SFE enables partial dislocation motion and martensitic transformation. Based on thermodynamic estimations and comparisons with similar HEA systems (e.g., CoCrFeMnNi), the SFE of the studied alloy is expected to fall in the range of 15–25 mJ/m² at room temperature near the threshold between twinning and transformation regimes.

As temperature decreases, the SFE tends to decline further, lowering the energetic barrier for FCC-to-BCC transformation and thereby amplifying TRIP activity. This trend is evident in the experimental results: the extent of BCC phase formation increased significantly as the temperature dropped from 400 °C to −196 °C. At cryogenic conditions, the reduced SFE facilitated the formation of thick stacking faults and local lattice instabilities, creating favorable conditions for nucleation and growth of the BCC phase.

At elevated temperatures (400 °C), the SFE rises, stabilizing the FCC phase and suppressing transformation. This was reflected in the XRD and EBSD analyses, which showed minimal BCC formation and signs of thermal recovery. The mechanical response also shifted toward conventional dislocation-driven softening and reduced strain hardening, confirming the inactivity of the TRIP mechanism in this regime.

The alloy's multi-element composition comprising Fe, Mn, Co, Cr, and Ni introduces significant atomic size mismatch and chemical disorder. This complexity gives rise to severe lattice distortion, which has a dual effect: it enhances solid solution strengthening and promotes mechanical instability in the FCC phase. Lattice distortion contributes to the transformation driving force by altering the Gibbs free energy difference (ΔG) between the FCC and BCC phases. The distortion energy component can be estimated by the following relation:

$$\Delta \mathrm{E}_{dist} \propto \sum c_i (r_i - \bar{r}_i)^2 \quad (4.1)$$

where c_i is the atomic fraction of element i,r_i is its atomic radius, and $\bar{r}_i$ is the average atomic radius of the alloy. A higher distortion energy destabilizes the FCC phase, making it more prone to stress- or strain-induced transformation. Moreover, the presence of high configurational entropy and chemical disorder delays recovery and dynamic recrystallization, allowing deformation-induced structures to persist longer further contributing to dislocation accumulation and transformation activation An important microstructural feature enabling the TRIP effect in the annealed condition is the dual-phase structure comprising soft FCC and hard BCC regions. This heterogeneity facilitates strain partitioning during deformation, with the FCC matrix accommodating most of the plastic strain and the harder BCC regions acting as load-bearing zones.

As deformation progresses, localized stress concentrations develop near phase boundaries, grain boundaries, and triple junctions sites where BCC nucleation is often initiated. The growth of BCC regions during loading introduces additional phase boundaries and increases dislocation storage, particularly in the form of geometrically necessary dislocations (GNDs). EBSD KAM and GND maps confirmed this behavior, revealing strong correlations between high misorientation zones and BCC-rich areas.
This feedback loop between transformation, dislocation hardening, and microstructural refinement results in sustained strain hardening over a broad range of plastic strains. It also enhances back-stress development and contributes to the observed strength–ductility synergy at low temperatures.

4.5 Correlation Between Microstructure and Mechanical Behavior

The mechanical response of TRIP-assisted high-entropy alloys (HEAs) is intricately linked to their evolving microstructure during plastic deformation. In this study, EBSD and XRD analyses were systematically combined with tensile testing across −196 °C, 25 °C, and 400 °C to elucidate how microstructural features such as phase fraction, grain size, dislocation structure, and transformation activity collectively influence mechanical performance. At cryogenic temperatures, the alloy displayed its most outstanding mechanical behavior. The annealed condition reached a true ultimate tensile strength of ~1603 MPa with ~20% elongation, while the as-received sample yielded at 448 MPa and fractured at 1273 MPa. The superior response in the annealed state can be directly traced to its microstructural characteristics. EBSD and XRD confirmed substantial FCC-to-BCC phase transformation during deformation, with BCC content increasing from ~6% to ~25% [104,105]. This robust TRIP activation significantly enhanced strain partitioning by forming a dynamically evolving dual-phase structure, which delayed necking and facilitated uniform deformation. In parallel, the dislocation landscape also transformed considerably. EBSD KAM maps revealed sharp misorientation gradients, especially along grain boundaries and shear bands. The GND density increased from $\sim 157 \times 10^{12}\ m^{-2}$ to over $250 \times 10^{12}\ m^{-2}$, indicating intense dislocation storage. The presence of high GND concentrations, distributed both near interfaces and within grain interiors, points to a microstructure capable of accommodating strain heterogeneously an ideal condition for sustained hardening. The annealed condition's fine-grained, metastable microstructure with pre-existing BCC regions and high initial GND density created favorable conditions for TRIP-induced plasticity and back-stress formation, leading to the observed synergy between strength and ductility.

In contrast, the as-received condition, with a coarse-grained FCC matrix and lower dislocation density, also benefitted from reduced SFE at cryogenic temperatures. As the temperature dropped from 400 °C to −196 °C, its yield strength, UTS, and fracture strain increased by 80%, 90%, and 24.5%, respectively. This mechanical improvement was largely dislocation-driven due to the suppression of dynamic recovery and enhanced storage of SSDs, though TRIP contribution remained limited. At ambient temperature, the mechanical behavior of both microstructures remained favorable, but the distinction between them persisted. The annealed samples achieved a UTS of ~1100 MPa with ~10% elongation, while TRIP activity continued, albeit at a lower rate. EBSD phase maps showed a rise in BCC content to ~18% post-deformation, suggesting ongoing transformation in high-strain regions such as shear bands and grain junctions. The as-received samples also showed a strength–ductility balance, but less pronounced. In the annealed condition, localized stress promoted partial FCC to BCC transformation, while the fine-grained microstructure provided more nucleation sites. Simultaneously, the accumulation of GNDs and SSDs in grain interiors and near GNBs contributed to back-stress hardening. The combined effect of dislocation storage and moderate TRIP activity resulted in a well-balanced mechanical response. However, due to the inherently higher dislocation density in the annealed condition (originating from prior cold rolling), elongation remained somewhat lower than in the as-received state at this temperature[25,106].

Tensile testing at 400 °C revealed a distinct drop in mechanical performance. The annealed condition still showed higher strength (~850 MPa UTS) compared to the as-received state, yet both experienced lower elongation (~8% for annealed). This degradation in performance was linked to the suppression of the TRIP effect at high

temperatures. XRD and EBSD analyses indicated that the FCC matrix remained largely stable, with only a marginal BCC fraction increase (from ~6% to ~9%). The higher SFE at elevated temperatures stabilized the FCC phase, diminishing the driving force for transformation. Additionally, thermally activated mechanisms such as dislocation climb and dynamic recovery reduced dislocation density. EBSD GND maps and KAM values supported this observation, showing less pronounced misorientation and reduced GND accumulation. The result was a more homogeneous deformation mode governed mainly by dislocation glide and recovery, leading to diffuse plastic flow with limited work hardening. Despite this, the annealed condition maintained more than double the yield strength compared to the as-received condition, highlighting the continued contribution of finer grain structure and higher initial GND density even in the absence of strong TRIP activity [107,108].

4.6 Strain Hardening Behavior

Strain hardening behavior was analyzed using true stress strain curves and calculated Strain Hardening Rate (SHR) plots at −196 °C, 25 °C, and 400 °C for both microstructural conditions (see Figure 3.1). These plots reveal strong temperature dependence and highlight how microstructure influences the strain hardening response through both dislocation activity and deformation-induced phase transformation.

At cryogenic temperature, the annealed alloy exhibited a markedly enhanced SHR throughout the deformation process. The SHR curve featured a prolonged plateau, indicating sustained work hardening, followed by a gradual decline only near the onset of necking. This elevated hardening capacity can be attributed to the synergistic action of several mechanisms. First, dynamic recovery was largely suppressed at low temperatures,

enabling continuous accumulation of dislocations without annihilation. Second, the activation of the transformation-induced plasticity (TRIP) effect led to extensive FCC-to-BCC phase transformation, introducing new phase boundaries that acted as effective barriers to dislocation motion. Third, a significant buildup of Geometrically Necessary Dislocations (GNDs) was observed, particularly along grain boundary networks (GNBs) and within grain interiors, contributing to internal back-stress and additional strain hardening. Together, these mechanisms provided the alloy with excellent resistance to localized deformation and delayed the onset of plastic instability. The SHR plot featured a distinct kink at ~5% true strain in the annealed samples indicating the onset of transformation induced hardening. These peaks are primarily associated with the sudden activation of TRIP, where rapid phase transformation temporarily accelerates dislocation accumulation and strain hardening. In contrast, the as-received samples lack sufficient BCC nuclei and heterogeneous microstructural features, so the SHR remains smooth without pronounced peaks. This behavior underscores the dominant role of TRIP in enhancing strain hardening and enabling high strength (up to 1603 MPa) with sustained plasticity (~20% elongation). This behavior underscores the dominant role of TRIP in enhancing strain hardening and enabling high strength (up to 1603 MPa) with sustained plasticity (~20% elongation). The as-received condition also benefitted from suppressed recovery, but in the absence of significant TRIP, its hardening behavior was mainly governed by SSD storage and grain boundary interactions [36,80].

At room temperature, the SHR curve for the annealed condition remained robust, although less intense than at cryogenic temperatures. The kink in the SHR curve appeared at a slightly higher strain level, reflecting delayed but still active phase transformation. While the TRIP effect was partially diminished, its localized occurrence in high strain

zones contributed meaningfully to the hardening response. Dislocation glide, together with GND storage and partial phase transformation, collectively enhanced strain resistance. The as-received sample, lacking significant phase transformation or high initial GND content, exhibited a smoother SHR profile with reduced work hardening capacity compared to the annealed condition. At elevated temperatures, both the SHR and strain hardening capacity decreased sharply. For both material conditions, the SHR curve showed a rapid decline without the presence of a transformation induced kink. Instead, a plateau was observed, consistent with the absence of significant FCC to BCC transformation due to elevated SFE. In the annealed condition, some residual hardening was maintained due to the finer grain structure and higher GND density, but thermal activation of dislocation climb and dynamic recovery limited further accumulation. This led to an overall softening behavior with early plastic flow and reduced strength–ductility performance. In essence, the observed temperature-dependent trends in SHR reflect the complex interplay between microstructure, dislocation mechanics, and TRIP activity. The fine grained, heterogeneous annealed condition consistently achieved higher hardening rates and strength levels across all temperatures, with cryogenic conditions amplifying these effects through low SFE, high GND density, and vigorous transformation. The coarse-grained, single phase as-received condition, while responsive to low-temperature strengthening, lacked the same synergy and microstructural adaptability, resulting in a less pronounced hardening behavior [93,102].

5. Conclusion and Future Work

This study investigated the effect of deformation temperature on the mechanical behavior and transformation induced plasticity (TRIP) response of a dual-phase high-entropy alloy (HEA) composed of Fe, Mn, Co, Cr, and Ni. By applying a sequence of homogenization, cold rolling, and annealing, a tailored FCC-BCC microstructure was developed to activate TRIP and explore the role of phase metastability under cryogenic, ambient, and elevated temperatures. The combined use of mechanical testing, X-ray diffraction (XRD), and electron backscatter diffraction (EBSD) provided comprehensive insights into the interplay between phase transformation, dislocation behavior, and strain localization mechanisms.

1. The alloy exhibited temperature-sensitive TRIP activity, which directly influenced its mechanical performance. At −196 °C, the TRIP effect was strongly activated, as evidenced by a significant FCC-to-BCC transformation, resulting in a high ultimate tensile strength (~1600 MPa) and an elongation approaching 18%. This behavior was attributed to a pronounced reduction in stacking fault energy (SFE), which destabilized the FCC phase and promoted transformation under applied stress. At 25 °C, the transformation persisted in a more localized manner, continuing to enhance strain hardening, while at 400 °C, the TRIP effect was largely inactive due to increased SFE and the dominance of thermally activated recovery mechanisms.

2. EBSD-based strain mapping revealed that low-temperature deformation was accompanied by substantial dislocation accumulation and strain heterogeneity, particularly in the annealed condition. Kernel Average Misorientation (KAM) and geometrically necessary dislocation (GND) maps confirmed increased lattice distortion

at cryogenic temperatures, aligning with the activation of TRIP and its contribution to work hardening. In contrast, elevated temperature deformation showed reduced KAM and GND activity, consistent with dynamic recovery, dislocation annihilation, and the suppression of phase transformation.

3. The alloy's responsiveness to deformation-induced transformation was closely tied to its intrinsic lattice distortion and thermodynamic metastability. The severe atomic size mismatch among its constituent elements, coupled with moderate SFE, lowered the energy barrier for FCC-to-BCC transformation. These conditions created a favorable environment for stress-assisted martensitic nucleation and growth. The findings highlight the importance of atomic-scale design in tailoring transformation potential and mechanical properties in metastable HEAs.

4. The results of this study underscore the effectiveness of thermomechanical processing in tuning phase stability and deformation pathways without altering overall composition. The ability to trigger and control TRIP through structural manipulation offers a powerful strategy for designing high-strength, ductile, and thermally robust materials. These insights contribute to the broader understanding of deformation mechanisms in HEAs and establish a framework for the development of advanced structural materials that maintain mechanical performance across diverse service environments.

5. Looking ahead, future research should extend these findings to additive manufacturing (AM) approaches, particularly laser and beam based directed energy deposition (DED) and selective laser melting (SLM), where rapid solidification, high thermal gradients, and cyclic reheating are expected to further influence phase stability

and TRIP activity. Investigating the processing microstructure property relationships under AM conditions will not only enable the tailoring of site specific phase metastability but also reveal the scalability of TRIP assisted HEAs for complex geometries and critical structural applications. Moreover, exploring compositional variations and alloying strategies in other TRIP-assisted HEAs within the AM framework can provide deeper insight into the interplay between metastability, defect structures, and mechanical performance, ultimately guiding the design of next-generation high-performance alloys.

REFERENCES

[1] B. Cantor, I.T.H. Chang, P. Knight, A.J.B. Vincent, Microstructural development in equiatomic multicomponent alloys, Materials Science and Engineering A 375–377 (2004) 213–218. https://doi.org/10.1016/j.msea.2003.10.257.

[2] E.P. George, D. Raabe, R.O. Ritchie, High-entropy alloys, Nat Rev Mater 4 (2019) 515–534. https://doi.org/10.1038/s41578-019-0121-4.

[3] W. Li, D. Xie, D. Li, Y. Zhang, Y. Gao, P.K. Liaw, Mechanical behavior of high-entropy alloys, Prog Mater Sci 118 (2021). https://doi.org/10.1016/j.pmatsci.2021.100777.

[4] H.Y. Diao, R. Feng, K.A. Dahmen, P.K. Liaw, Fundamental deformation behavior in high-entropy alloys: An overview, Curr Opin Solid State Mater Sci 21 (2017) 252–266. https://doi.org/10.1016/j.cossms.2017.08.003.

[5] B. V, A.X. M, Development of high entropy alloys (HEAs): Current trends, Heliyon 10 (2024). https://doi.org/10.1016/j.heliyon.2024.e26464.

[6] H. Yu, J. Zhang, W. Fang, R. Chang, X. Bai, J. Yan, X. Zhang, B. Liu, F. Yin, A brief review of metastable high-entropy alloys with transformation-induced plasticity, Materials Science and Technology (United Kingdom) 36 (2020) 1893–1902. https://doi.org/10.1080/02670836.2020.1851437.

[7] M.S. Mehranpour, M.J. Sohrabi, A. Jalali, A. Kalhor, A. Heydarinia, M.Z. Aghdam, H. Mirzadeh, M. Malekan, H. Shahmir, K. Rodak, H.S. Kim, Coupling different strengthening mechanisms with transformation-induced plasticity (TRIP) effect in advanced high-entropy alloys: A comprehensive review, Materials Science and Engineering: A 926 (2025). https://doi.org/10.1016/j.msea.2025.147914.

[8] Z. Li, D. Raabe, Strong and Ductile Non-equiatomic High-Entropy Alloys: Design, Processing, Microstructure, and Mechanical Properties, JOM 69 (2017) 2099–2106. https://doi.org/10.1007/s11837-017-2540-2.

[9] D. Kumar, Recent advances in tribology of high entropy alloys: A critical review, Prog Mater Sci 136 (2023). https://doi.org/10.1016/j.pmatsci.2023.101106.

[10] A.O. Soto, A.S. Salgado, E.B. Niño, Thermodynamic analysis of high entropy alloys and their mechanical behavior in high and low-temperature conditions with a microstructural approach - A review, Intermetallics (Barking) 124 (2020). https://doi.org/10.1016/j.intermet.2020.106850.

[11] P.I. Odetola, B.J. Babalola, A.E. Afolabi, U.S. Anamu, E. Olorundaisi, M.C. Umba, T. Phahlane, O.O. Ayodele, P.A. Olubambi, Exploring high entropy alloys: A review on thermodynamic design and computational modeling strategies for

advanced materials applications, Heliyon 10 (2024). https://doi.org/10.1016/j.heliyon.2024.e39660.

[12] U.S. Anamu, O.O. Ayodele, E. Olorundaisi, B.J. Babalola, P.I. Odetola, A. Ogunmefun, K. Ukoba, T.C. Jen, P.A. Olubambi, Fundamental design strategies for advancing the development of high entropy alloys for thermo-mechanical application: A critical review, Journal of Materials Research and Technology 27 (2023) 4833–4860. https://doi.org/10.1016/j.jmrt.2023.11.008.

[13] D.B. Miracle, O.N. Senkov, A critical review of high entropy alloys and related concepts, Acta Mater 122 (2017) 448–511. https://doi.org/10.1016/j.actamat.2016.08.081.

[14] J.W. Yeh, Physical Metallurgy of High-Entropy Alloys, JOM 67 (2015) 2254–2261. https://doi.org/10.1007/s11837-015-1583-5.

[15] R. Li, L. Xie, W.Y. Wang, P.K. Liaw, Y. Zhang, High-Throughput Calculations for High-Entropy Alloys: A Brief Review, Front Mater 7 (2020). https://doi.org/10.3389/fmats.2020.00290.

[16] D. Chen, X. Zhu, X. Yang, N. Yan, Y. Cui, X. Lei, L. Liu, J. Khaliq, C. Li, A review on structure–property relationships in dielectric ceramics using high-entropy compositional strategies, Journal of the American Ceramic Society 106 (2023) 6602–6616. https://doi.org/10.1111/jace.19349.

[17] A.J. Zaddach, C. Niu, C.C. Koch, D.L. Irving, Mechanical properties and stacking fault energies of NiFeCrCoMn high-entropy alloy, JOM 65 (2013) 1780–1789. https://doi.org/10.1007/s11837-013-0771-4.

[18] Q. Lin, J. Liu, X. An, H. Wang, Y. Zhang, X. Liao, Cryogenic-deformation-induced phase transformation in an FeCoCrNi high-entropy alloy, Mater Res Lett 6 (2018) 236–243. https://doi.org/10.1080/21663831.2018.1434250.

[19] Q. Wang, Y. Lu, Q. Yu, Z. Zhang, The Exceptional Strong Face-centered Cubic Phase and Semi-coherent Phase Boundary in a Eutectic Dual-phase High Entropy Alloy AlCoCrFeNi, Sci Rep 8 (2018) 1–7. https://doi.org/10.1038/s41598-018-33330-0.

[20] C. Lee, G. Song, M.C. Gao, R. Feng, P. Chen, J. Brechtl, Y. Chen, K. An, W. Guo, J.D. Poplawsky, S. Li, A.T. Samaei, W. Chen, A. Hu, H. Choo, P.K. Liaw, Lattice distortion in a strong and ductile refractory high-entropy alloy, Acta Mater 160 (2018) 158–172. https://doi.org/10.1016/j.actamat.2018.08.053.

[21] D. Liu, Q. Yu, S. Kabra, M. Jiang, P. Forna-Kreutzer, R. Zhang, M. Payne, F. Walsh, B. Gludovatz, M. Asta, A.M. Minor, E.P. George, R.O. Ritchie, Exceptional fracture toughness of CrCoNi-based medium-and high-entropy alloys close to liquid helium temperatures, n.d.

[22] W. Li, P.K. Liaw, Y. Gao, Fracture resistance of high entropy alloys: A review, Intermetallics (Barking) 99 (2018) 69–83. https://doi.org/10.1016/j.intermet.2018.05.013.

[23] C. Varvenne, A. Luque, W.A. Curtin, Theory of strengthening in fcc high entropy alloys, Acta Mater 118 (2016) 164–176. https://doi.org/10.1016/j.actamat.2016.07.040.

[24] D. Ma, M. Yao, K.G. Pradeep, C.C. Tasan, H. Springer, D. Raabe, Phase stability of non-equiatomic CoCrFeMnNi high entropy alloys, Acta Mater 98 (2015) 288–296. https://doi.org/10.1016/j.actamat.2015.07.030.

[25] A. Lasalmonie, J.L. Strudel, Influence of grain size on the mechanical behaviour of some high strength materials, J Mater Sci 21 (1986) 1837–1852. https://doi.org/10.1007/BF00547918.

[26] J.W. Bae, J.B. Seol, J. Moon, S.S. Sohn, M.J. Jang, H.Y. Um, B.J. Lee, H.S. Kim, Exceptional phase-transformation strengthening of ferrous medium-entropy alloys at cryogenic temperatures, Acta Mater 161 (2018) 388–399. https://doi.org/10.1016/j.actamat.2018.09.057.

[27] G.H. Gu, S.G. Jeong, Y.-U. Heo, H. Ha, S.Y. Ahn, J.Y. Lee, J. Lee, S. Harjo, W. Gong, J. Cho, H.S. Kim, Temperature-dependent deformation behavior of dual-phase medium-entropy alloy: In-situ neutron diffraction study, J Mater Sci Technol (2025). https://doi.org/10.1016/j.jmst.2024.11.057.

[28] S.F. Liu, Y. Wu, H.T. Wang, J.Y. He, J.B. Liu, C.X. Chen, X.J. Liu, H. Wang, Z.P. Lu, Stacking fault energy of face-centered-cubic high entropy alloys, Intermetallics (Barking) 93 (2018) 269–273. https://doi.org/10.1016/j.intermet.2017.10.004.

[29] Z. Qiu, C. Yao, K. Feng, Z. Li, P.K. Chu, Cryogenic deformation mechanism of CrMnFeCoNi high-entropy alloy fabricated by laser additive manufacturing process, International Journal of Lightweight Materials and Manufacture 1 (2018) 33–39. https://doi.org/10.1016/j.ijlmm.2018.02.001.

[30] X. Wen, L. Zhu, M. Naeem, H. Huang, S. Jiang, H. Wang, X. Liu, X. Zhang, X.L. Wang, Y. Wu, Z. Lu, Strong work-hardenable body-centered-cubic high-entropy alloys at cryogenic temperature, Scr Mater 231 (2023). https://doi.org/10.1016/j.scriptamat.2023.115434.

[31] Q. Ding, X. Fu, D. Chen, H. Bei, B. Gludovatz, J. Li, Z. Zhang, E.P. George, Q. Yu, T. Zhu, R.O. Ritchie, Real-time nanoscale observation of deformation mechanisms in CrCoNi-based medium- to high-entropy alloys at cryogenic temperatures, Materials Today 25 (2019) 21–27. https://doi.org/10.1016/j.mattod.2019.03.001.

[32] S. Martin, S. Wolf, U. Martin, L. Krüger, D. Rafaja, Deformation Mechanisms in Austenitic TRIP/TWIP Steel as a Function of Temperature, Metall Mater Trans A

Phys Metall Mater Sci 47 (2016) 49–58. https://doi.org/10.1007/s11661-014-2684-4.

[33] T.Z. Khan, T. Kirk, G. Vazquez, P. Singh, A. V. Smirnov, D.D. Johnson, K. Youssef, R. Arróyave, Towards stacking fault energy engineering in FCC high entropy alloys, Acta Mater 224 (2022). https://doi.org/10.1016/j.actamat.2021.117472.

[34] N. Stepanov, M. Tikhonovsky, N. Yurchenko, D. Zyabkin, M. Klimova, S. Zherebtsov, A. Efimov, G. Salishchev, Effect of cryo-deformation on structure and properties of CoCrFeNiMn high-entropy alloy, Intermetallics (Barking) 59 (2015) 8–17. https://doi.org/10.1016/j.intermet.2014.12.004.

[35] P. Wu, Y. Zhang, L. Han, K. Gan, D. Yan, W. Wu, L. He, Z. Fu, Z. Li, Unexpected sluggish martensitic transformation in a strong and super-ductile high-entropy alloy of ultralow stacking fault energy, Acta Mater 261 (2023). https://doi.org/10.1016/j.actamat.2023.119389.

[36] S. Huang, W. Li, S. Lu, F. Tian, J. Shen, E. Holmström, L. Vitos, Temperature dependent stacking fault energy of FeCrCoNiMn high entropy alloy, Scr Mater 108 (2015) 44–47. https://doi.org/10.1016/j.scriptamat.2015.05.041.

[37] H. Chang, T. Zhang, Z. Li, J. Ma, J. Wang, D. Zhao, S. Ma, Z. Wang, Cryogenic mechanical behavior and FCC → HCP phase transformation mechanism in a Si-added CrCoNi medium-entropy alloy under quasi-static and dynamic tension, Mater Des 244 (2024). https://doi.org/10.1016/j.matdes.2024.113131.

[38] Y.H. Jo, S. Jung, W.M. Choi, S.S. Sohn, H.S. Kim, B.J. Lee, N.J. Kim, S. Lee, Cryogenic strength improvement by utilizing room-temperature deformation twinning in a partially recrystallized VCrMnFeCoNi high-entropy alloy, Nat Commun 8 (2017). https://doi.org/10.1038/ncomms15719.

[39] M. Naeem, R.J. Sánchez Cruz, M.A. Esquivel Neri, Y. Ma, V. Amigó Borrás, G. González, A.J. Knowles, W. Gong, S. Harjo, Y.T. Zhu, X.-L. Wang, L. Romero-Resendiz, Enhanced cryogenic mechanical properties of heterostructured CrCoNi multicomponent alloy: Insights from in-situ neutron diffraction, Materials Science and Engineering: A 916 (2024) 147374. https://doi.org/10.1016/j.msea.2024.147374.

[40] B. Gludovatz, A. Hohenwarter, K.V.S. Thurston, H. Bei, Z. Wu, E.P. George, R.O. Ritchie, Exceptional damage-tolerance of a medium-entropy alloy CrCoNi at cryogenic temperatures, Nat Commun 7 (2016). https://doi.org/10.1038/ncomms10602.

[41] D. Lin, L. Xu, Y. Han, Y. Zhang, H. Jing, L. Zhao, F. Minami, Structure and mechanical properties of a FeCoCrNi high-entropy alloy fabricated via selective laser melting, Intermetallics (Barking) 127 (2020). https://doi.org/10.1016/j.intermet.2020.106963.

[42] H. Yi, C. Tao, C. Chen, J. Fan, S. Wang, Enhanced cryogenic tensile properties in a Fe-high-entropy alloy, J Alloys Compd 1017 (2025) 179052. https://doi.org/10.1016/j.jallcom.2025.179052.

[43] Q.X. Ma, H.J. Yang, Z. Wang, X.H. Shi, P.K. Liaw, J.W. Qiao, High strength and ductility in partially recrystallized Fe40Mn20Cr20Ni20 high-entropy alloys at cryogenic temperature, Microstructures 2 (2022). https://doi.org/10.20517/microstructures.2022.12.

[44] H. Yi, C. Tao, C. Chen, J. Fan, S. Wang, Enhanced cryogenic tensile properties in a Fe-high-entropy alloy, J Alloys Compd 1017 (2025) 179052. https://doi.org/10.1016/j.jallcom.2025.179052.

[45] D. Zhou, C. Shi, C. Wang, R. Sheng, W. Li, Y. Tong, Tensile Properties of a Non-Equiatomic Ni–Co–V Medium Entropy Alloy at Cryogenic Temperature, Metals (Basel) 14 (2024). https://doi.org/10.3390/met14050590.

[46] X. Wang, Z. Zhang, Z. Wang, X. Ren, Microstructural Evolution and Tensile Properties of Al0.3CoCrFeNi High-Entropy Alloy Associated with B2 Precipitates, Materials 15 (2022). https://doi.org/10.3390/ma15031215.

[47] S. She, C. Wang, M. Chen, V. Ji, Mechanical Properties and Strengthening Mechanisms of FCC-Based and Refractory High-Entropy Alloys: A Review, Metals (Basel) 15 (2025). https://doi.org/10.3390/met15030247.

[48] V.A.S. Kondapalli, K. Suresh, M. Ramakrishna, N. Narasaiah, B. Srinivasarao, Effect of Cu content on the microstructure and mechanical properties of FeNiMnCuxAl0.1Ti0.1 (x = 0.5,1.0 and 1.5) high entropy alloy system, J Alloys Compd 940 (2023). https://doi.org/10.1016/j.jallcom.2023.168819.

[49] W.H. Liu, J.Y. He, H.L. Huang, H. Wang, Z.P. Lu, C.T. Liu, Effects of Nb additions on the microstructure and mechanical property of CoCrFeNi high-entropy alloys, Intermetallics (Barking) 60 (2015) 1–8. https://doi.org/10.1016/j.intermet.2015.01.004.

[50] J.Y. He, C. Zhu, D.Q. Zhou, W.H. Liu, T.G. Nieh, Z.P. Lu, Steady state flow of the FeCoNiCrMn high entropy alloy at elevated temperatures, Intermetallics (Barking) 55 (2014) 9–14. https://doi.org/10.1016/j.intermet.2014.06.015.

[51] P. Wu, K. Gan, D. Yan, Z. Li, The temperature dependence of deformation behaviors in high-entropy alloys: A review, Metals (Basel) 11 (2021). https://doi.org/10.3390/met11122005.

[52] W.R. Wang, W.L. Wang, J.W. Yeh, Phases, microstructure and mechanical properties of AlxCoCrFeNi high-entropy alloys at elevated temperatures, J Alloys Compd 589 (2014) 143–152. https://doi.org/10.1016/j.jallcom.2013.11.084.

[53] S. Wang, M. Wu, D. Shu, G. Zhu, D. Wang, B. Sun, Mechanical instability and tensile properties of TiZrHfNbTa high entropy alloy at cryogenic temperatures, Acta Mater 201 (2020) 517–527. https://doi.org/10.1016/j.actamat.2020.10.044.

[54] W. Jiang, S. Yuan, Y. Cao, Y. Zhang, Y. Zhao, Mechanical properties and deformation mechanisms of a Ni2Co1Fe1V0.5Mo0.2 medium-entropy alloy at elevated temperatures, Acta Mater 213 (2021). https://doi.org/10.1016/j.actamat.2021.116982.

[55] S.P. Akula, M. Ojha, K.L. Rao, A.K. Gupta, A review on superplastic forming of Ti-6Al-4V and other titanium alloys, Mater Today Commun 34 (2023). https://doi.org/10.1016/j.mtcomm.2023.105343.

[56] O.N. Senkov, G.B. Wilks, D.B. Miracle, C.P. Chuang, P.K. Liaw, Refractory high-entropy alloys, Intermetallics (Barking) 18 (2010) 1758–1765. https://doi.org/10.1016/j.intermet.2010.05.014.

[57] A.K. Chandan, K. Kishore, P.T. Hung, M. Ghosh, S.G. Chowdhury, M. Kawasaki, J. Gubicza, Effect of nickel addition on enhancing nano-structuring and suppressing TRIP effect in Fe40Mn40Co10Cr10 high entropy alloy during high-pressure torsion, Int J Plast 150 (2022). https://doi.org/10.1016/j.ijplas.2021.103193.

[58] E. Jimenez-Melero, N.H. van Dijk, L. Zhao, J. Sietsma, S.E. Offerman, J.P. Wright, S. van der Zwaag, The effect of aluminium and phosphorus on the stability of individual austenite grains in TRIP steels, Acta Mater 57 (2009) 533–543. https://doi.org/10.1016/j.actamat.2008.09.040.

[59] W. Fu, W. Zheng, Y. Huang, F. Guo, S. Jiang, P. Xue, Y. Ren, H. Fan, Z. Ning, J. Sun, Cryogenic mechanical behaviors of CrMnFeCoNi high-entropy alloy, Materials Science and Engineering: A 789 (2020). https://doi.org/10.1016/j.msea.2020.139579.

[60] Z. Li, K.G. Pradeep, Y. Deng, D. Raabe, C.C. Tasan, Metastable high-entropy dual-phase alloys overcome the strength-ductility trade-off, Nature 534 (2016) 227–230. https://doi.org/10.1038/nature17981.

[61] R. Zhang, S. Zhao, J. Ding, Y. Chong, T. Jia, C. Ophus, M. Asta, R.O. Ritchie, A.M. Minor, Short-range order and its impact on the CrCoNi medium-entropy alloy, Nature 581 (2020) 283–287. https://doi.org/10.1038/s41586-020-2275-z.

[62] W.R. Wang, W.L. Wang, S.C. Wang, Y.C. Tsai, C.H. Lai, J.W. Yeh, Effects of Al addition on the microstructure and mechanical property of Al xCoCrFeNi high-entropy alloys, Intermetallics (Barking) 26 (2012) 44–51. https://doi.org/10.1016/j.intermet.2012.03.005.

[63] Z. Cao, H. Chen, W. Wang, J. Guo, Z. Sun, Y. Hai, W. Yin, Effect of Ti content on the microstructure and mechanical properties of TixZrNbMoV lightweight refractory high-entropy alloys, Int J Refract Metals Hard Mater 119 (2024). https://doi.org/10.1016/j.ijrmhm.2023.106547.

[64] E.W. Huang, H.S. Chou, K.N. Tu, W.S. Hung, T.N. Lam, C.W. Tsai, C.Y. Chiang, B.H. Lin, A.C. Yeh, S.H. Chang, Y.J. Chang, J.J. Yang, X.Y. Li, C.S. Ku, K. An,

Y.W. Chang, Y.L. Jao, Element Effects on High-Entropy Alloy Vacancy and Heterogeneous Lattice Distortion Subjected to Quasi-equilibrium Heating, Sci Rep 9 (2019) 1–10. https://doi.org/10.1038/s41598-019-51297-4.

[65] Y. Zhou, D. Zhou, X. Jin, L. Zhang, X. Du, B. Li, Design of non-equiatomic medium-entropy alloys, Sci Rep 8 (2018). https://doi.org/10.1038/s41598-018-19449-0.

[66] X. Liu, M. Nakatani, H. Gao, B. Sharma, H. Pan, Z. Fu, X. Li, K. Ameyama, X. Zhu, Effect of stacking fault energy on deformation mechanisms in Cu and Cu-30% Zn alloy with gradient structure obtained by SMAT, J Alloys Compd 865 (2021). https://doi.org/10.1016/j.jallcom.2021.158863.

[67] C. Wagner, E.P. George, G. Laplanche, Effects of grain size and stacking fault energy on twinning stresses of single-phase CrxMn20Fe20Co20Ni40-x high-entropy alloys, Acta Mater 282 (2025). https://doi.org/10.1016/j.actamat.2024.120470.

[68] Z. Li, K.G. Pradeep, Y. Deng, D. Raabe, C.C. Tasan, Metastable high-entropy dual-phase alloys overcome the strength-ductility trade-off, Nature 534 (2016) 227–230. https://doi.org/10.1038/nature17981.

[69] Z. Li, C.C. Tasan, K.G. Pradeep, D. Raabe, A TRIP-assisted dual-phase high-entropy alloy: Grain size and phase fraction effects on deformation behavior, Acta Mater 131 (2017) 323–335. https://doi.org/10.1016/j.actamat.2017.03.069.

[70] R. Article, A REVIEW ON DEFORMATION STUDIES OF ALUMINUM ALLOYS PROCESSED THROUGH EQUAL CHANNEL ANGULAR PRESSING, (n.d.).

[71] A.M. Hossain, N. Kumar, Microstructure and mechanical properties of a dual phase transformation induced plasticity Fe-Mn-Co-Cr high entropy alloy, J Alloys Compd 893 (2022). https://doi.org/10.1016/j.jallcom.2021.162152.

[72] P. Shi, W. Ren, T. Zheng, Z. Ren, X. Hou, J. Peng, P. Hu, Y. Gao, Y. Zhong, P.K. Liaw, Enhanced strength–ductility synergy in ultrafine-grained eutectic high-entropy alloys by inheriting microstructural lamellae, Nat Commun 10 (2019) 1–8. https://doi.org/10.1038/s41467-019-08460-2.

[73] I.S. Wani, T. Bhattacharjee, S. Sheikh, Y.P. Lud, S. Chatterjee, P.P. Bhattacharjeea, S. Guo, N. Tsujib, Ultrafine-grained AlCoCrFeNi2.1 eutectic high-entropy alloy, Mater Res Lett 4 (2016) 174–179. https://doi.org/10.1080/21663831.2016.1160451.

[74] M. Delincé, Y. Bréchet, J.D. Embury, M.G.D. Geers, P.J. Jacques, T. Pardoen, Structure-property optimization of ultrafine-grained dual-phase steels using a microstructure-based strain hardening model, Acta Mater 55 (2007) 2337–2350. https://doi.org/10.1016/j.actamat.2006.11.029.

[75] A. Lasalmonie, J.L. Strudel, Review Influence of grain size on the mechanical behaviour of some high strength materials, 1986.

[76] S. Qin, M. Yang, P. Jiang, F. Yuan, X. Wu, Excellent tensile properties induced by heterogeneous grain structure and dual nanoprecipitates in high entropy alloys, Mater Charact 186 (2022) 111779. https://doi.org/10.1016/j.matchar.2022.111779.

[77] Z. Li, C.C. Tasan, K.G. Pradeep, D. Raabe, A TRIP-assisted dual-phase high-entropy alloy: Grain size and phase fraction effects on deformation behavior, Acta Mater 131 (2017) 323–335. https://doi.org/10.1016/j.actamat.2017.03.069.

[78] S.F. Liu, Y. Wu, H.T. Wang, J.Y. He, J.B. Liu, C.X. Chen, X.J. Liu, H. Wang, Z.P. Lu, Stacking fault energy of face-centered-cubic high entropy alloys, Intermetallics (Barking) 93 (2018) 269–273. https://doi.org/10.1016/j.intermet.2017.10.004.

[79] T. Zheng, J. Lv, Y. Wu, H.-H. Wu, S. Liu, J. Tang, M. Zhou, H. Wang, X. Liu, S. Jiang, Z. Lu, Effects of stacking fault energy on the deformation behavior of CoNiCrFeMn high-entropy alloys: A molecular dynamics study, Appl Phys Lett 119 (2021) 201907. https://doi.org/10.1063/5.0069108.

[80] D. Molnár, X. Sun, S. Lu, W. Li, G. Engberg, L. Vitos, Materials Science & Engineering A E ff ect of temperature on the stacking fault energy and deformation behaviour in 316L austenitic stainless steel, Materials Science & Engineering A 759 (2019) 490–497. https://doi.org/10.1016/j.msea.2019.05.079.

[81] C. Wagner, G. Laplanche, Acta Materialia Effects of stacking fault energy and temperature on grain boundary strengthening , intrinsic lattice strength and deformation mechanisms in CrMnFeCoNi high-entropy alloys with different Cr / Ni ratios, Acta Mater 244 (2023) 118541. https://doi.org/10.1016/j.actamat.2022.118541.

[82] S. Chen, H.S. Oh, B. Gludovatz, S.J. Kim, E.S. Park, Z. Zhang, R.O. Ritchie, Q. Yu, Real-time observations of TRIP-induced ultrahigh strain hardening in a dual-phase CrMnFeCoNi high-entropy alloy, Nat Commun 11 (2020). https://doi.org/10.1038/s41467-020-14641-1.

[83] W. Skrotzki, G. Dan Sathiaraj, R. Kalsar, S. Suwas, Effect of stacking fault energy on microstructure and texture evolution during the rolling of non-equiatomic crmnfeconi high-entropy alloys, Crystals (Basel) 10 (2020) 1–12. https://doi.org/10.3390/cryst10070607.

[84] Q. He, Y. Yang, On lattice distortion in high entropy alloys, Front Mater 5 (2018). https://doi.org/10.3389/fmats.2018.00042.

[85] S. Liu, Y. Wei, The Gaussian distribution of lattice size and atomic level heterogeneity in high entropy alloys, Extreme Mech Lett 11 (2017) 84–88. https://doi.org/10.1016/j.eml.2016.10.007.

[86] S. Qiu, X.C. Zhang, J. Zhou, S. Cao, H. Yu, Q.M. Hu, Z. Sun, Influence of lattice distortion on stacking fault energies of CoCrFeNi and Al-CoCrFeNi high entropy alloys, J Alloys Compd 846 (2020). https://doi.org/10.1016/j.jallcom.2020.156321.

[87] Z.G. Zhu, K.H. Ma, Q. Wang, C.H. Shek, Compositional dependence of phase formation and mechanical properties in three CoCrFeNi-(Mn/Al/Cu) high entropy alloys, Intermetallics (Barking) 79 (2016) 1–11. https://doi.org/10.1016/j.intermet.2016.09.003.

[88] Y. Liu, M. Xu, L. Xiao, X. Chen, Z. Hu, B. Gao, N. Liang, Y. Zhu, Y. Cao, H. Zhou, Dislocation array reflection enhances strain hardening of a dual-phase heterostructured high-entropy alloy, Mater Res Lett 11 (2023) 638–647. https://doi.org/10.1080/21663831.2023.2208166.

[89] G.K. Williamsont, W.H. Hallt, X-RAY LINE BROADENING FROM FILED ALUMINIUM AND WOLFRAM*, n.d.

[90] H. Mughrabi, Dual role of deformation-induced geometrically necessary dislocations with respect to lattice plane misorientations and/or long-range internal stresses, Acta Mater 54 (2006) 3417–3427. https://doi.org/10.1016/j.actamat.2006.03.047.

[91] D.A. Hughes, N. Hansen, D.J. Bammann, Geometrically necessary boundaries, incidental dislocation boundaries and geometrically necessary dislocations, n.d. www.actamat-journals.com.

[92] A. Kundu, D.P. Field, Influence of plastic deformation heterogeneity on development of geometrically necessary dislocation density in dual phase steel, Materials Science and Engineering: A 667 (2016) 435–443. https://doi.org/10.1016/j.msea.2016.05.022.

[93] J. Yang, Y.H. Jo, D.W. Kim, W.M. Choi, H.S. Kim, B.J. Lee, S.S. Sohn, S. Lee, Effects of transformation-induced plasticity (TRIP) on tensile property improvement of Fe45Co30Cr10V10Ni5-xMnx high-entropy alloys, Materials Science and Engineering: A 772 (2020). https://doi.org/10.1016/j.msea.2019.138809.

[94] L. Remy, Kinetics of Strain-Induced fcc • hcp Martensitic Transformation, 1977.

[95] H. Shahmir, P. Asghari-Rad, M.S. Mehranpour, F. Forghani, H.S. Kim, M. Nili-Ahmadabadi, Evidence of FCC to HCP and BCC-martensitic transformations in a CoCrFeNiMn high-entropy alloy by severe plastic deformation, Materials Science and Engineering: A 807 (2021). https://doi.org/10.1016/j.msea.2021.140875.

[96] B.G. I Taylor, R. Society Yarrow Professor, The Mechanism of Plastic Deformation of Crystals. Part I.-Theoretical, n.d. https://royalsocietypublishing.org/.

[97] W.D. Nix*$, H. Gao, INDENTATION SIZE EFFECTS IN CRYSTALLINE MATERIALS : A LAW FOR STRAIN GRADIENT PLASTICITY, 1998.

[98] S. Birosca, G. Liu, R. Ding, J. Jiang, T. Simm, C. Deen, M. Whittaker, The dislocation behaviour and GND development in a nickel based superalloy during creep, Int J Plast 118 (2019) 252–268. https://doi.org/10.1016/j.ijplas.2019.02.015.

[99] D.B. Miracle, O.N. Senkov, A critical review of high entropy alloys and related concepts, Acta Mater 122 (2017) 448–511. https://doi.org/10.1016/j.actamat.2016.08.081.

[100] A. Radi, P. Asghari-Rad, H.S. Kim, G.G. Yapici, On the development of a novel multi-phase high entropy alloy with transformation-induced plasticity effect, J Alloys Compd 905 (2022). https://doi.org/10.1016/j.jallcom.2022.164014.

[101] B.E. MacDonald, Z. Fu, B. Zheng, W. Chen, Y. Lin, F. Chen, L. Zhang, J. Ivanisenko, Y. Zhou, H. Hahn, E.J. Lavernia, Recent Progress in High Entropy Alloy Research, Jom 69 (2017) 2024–2031. https://doi.org/10.1007/s11837-017-2484-6.

[102] Z.Y. You, Z.Y. Tang, F.B. Chu, L. Ma, G.F. Guan, H. Ding, R.D.K. Misra, Microstructural design and deformation behavior of a TRIP/TWIP tri-phase heterogeneous high-entropy alloy, Intermetallics (Barking) 156 (2023). https://doi.org/10.1016/j.intermet.2023.107854.

[103] Z. Yang, D. Yan, W. Lu, Z. Li, A TWIP-TRIP quinary high-entropy alloy: Tuning phase stability and microstructure for enhanced mechanical properties, Materials Science and Engineering A 801 (2021) 140441. https://doi.org/10.1016/j.msea.2020.140441.

[104] Y.R. Wen, Y.P. Li, A. Hirata, Y. Zhang, T. Fujita, T. Furuhara, C.T. Liu, A. Chiba, M.W. Chen, Synergistic alloying effect on microstructural evolution and mechanical properties of Cu precipitation-strengthened ferritic alloys, Acta Mater 61 (2013) 7726–7740. https://doi.org/10.1016/j.actamat.2013.09.011.

[105] Y. Bai, H. Jiang, K. Yan, M. Li, Y. Wei, K. Zhang, B. Wei, Phase transition and heterogeneous strengthening mechanism in CoCrFeNiMn high-entropy alloy fabricated by laser-engineered net shaping via annealing at intermediate-temperature, J Mater Sci Technol 92 (2021) 129–137. https://doi.org/10.1016/j.jmst.2021.03.028.

[106] S.J. Sun, Y.Z. Tian, H.R. Lin, X.G. Dong, Y.H. Wang, Z.J. Wang, Z.F. Zhang, Temperature dependence of the Hall–Petch relationship in CoCrFeMnNi high-entropy alloy, J Alloys Compd 806 (2019) 992–998. https://doi.org/10.1016/j.jallcom.2019.07.357.

[107] R.M. Latanision, A.W. Ruff, The temperature dependence of stacking fault energy in Fe-Cr-Ni alloys, Metallurgical Transactions 2 (1971) 505–509. https://doi.org/10.1007/BF02663341.

[108] S. Curtze, V.T. Kuokkala, Dependence of tensile deformation behavior of TWIP steels on stacking fault energy, temperature and strain rate, Acta Mater 58 (2010) 5129–5141. https://doi.org/10.1016/j.actamat.2010.05.049.